

# Simplex Clustering via sBeta with Applications to Online Adjustment of Black-Box Predictions

Florent Chiaroni, Malik Boudiaf, Amar Mitiche and Ismail Ben Ayed

**Abstract**—We explore clustering the softmax predictions of deep neural networks and introduce a novel probabilistic clustering method, referred to as  $\kappa$ -SBETAS. In the general context of clustering discrete distributions, the existing methods focused on exploring distortion measures tailored to simplex data, such as the KL divergence, as alternatives to the standard Euclidean distance. We provide a general maximum a posteriori (MAP) perspective of clustering distributions, which emphasizes that the statistical models underlying the existing distortion-based methods may not be descriptive enough. Instead, we optimize a mixed-variable objective measuring the conformity of data within each cluster to the introduced sBeta density function, whose parameters are constrained and estimated jointly with binary assignment variables. Our versatile formulation approximates a variety of parametric densities for modeling simplex data, and enables to control the cluster-balance bias. This yields highly competitive performances for unsupervised adjustments of black-box model predictions in a variety of scenarios. Our code and comparisons with the existing simplex-clustering approaches along with our introduced softmax-prediction benchmarks are publicly available: [https://github.com/fchiaroni/Clustering\\_Softmax\\_Predictions](https://github.com/fchiaroni/Clustering_Softmax_Predictions).

**Index Terms**—Simplex clustering, softmax predictions, deep black-box models, unsupervised adjustments.

## 1 INTRODUCTION

OVER the last decade, deep neural networks have continuously gained wide interest for the semantic analysis of real-world data [2], [3]. However, under real-world conditions, potential feature or class distribution shifts of the target data may affect the predictive performances of pre-trained source models [4]. To address this issue, several recent adaptation approaches investigated fine-tuning all or a part of the model parameters using standard gradient-descent and back-propagation procedures [5], [6], [7]. However, in a breadth of practical applications [8], e.g. real-time predictions, it might be cumbersome to perform multiple forward and backward passes, more so when dealing with large (and continuously growing) deep-network models [9]. This may be the case even for adaptation methods that fine-tune only parts of the models, such as the parameters of the normalization layers [5]. More importantly, there are increasing concerns about both data privacy [10] and model-parameters inaccessibility [11]. In fact, the existing adaptation techniques assume knowledge of the source model and training procedures of the source training, which may not always hold in practice. Thus, off-the-shelf, model-agnostic solutions that mitigate the above concerns would be of interest in numerous real-world applications. In this work, we explore online unsupervised adjustment of softmax predictions from black-box source models, where we have access only to the model predictions. Specifically, we tackle the clustering of discrete distributions, with a particular focus on the output soft predictions from deep networks. Fig. 1

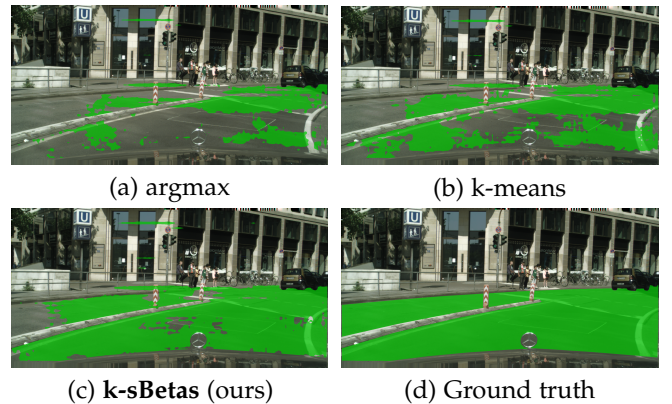
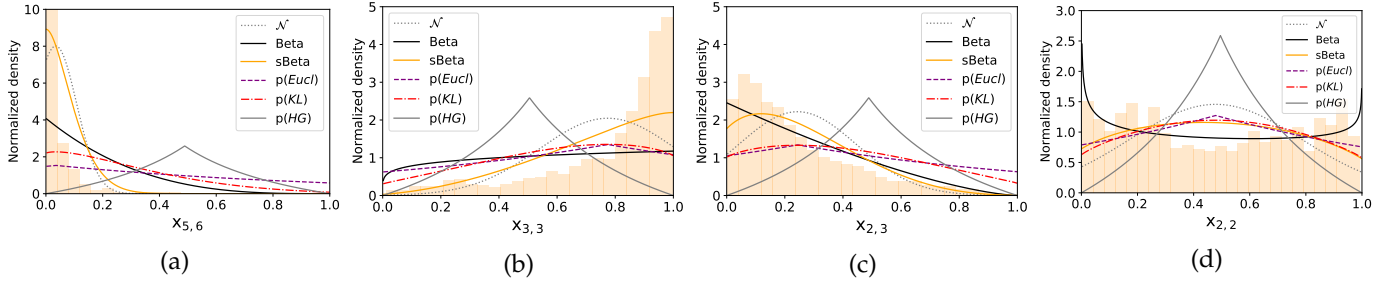


Fig. 1: **Real-time** (45 fps) unsupervised adjustment for road segmentation on images of size 2048x1024 using clustering on softmax predictions from a black-box source model, pre-trained on GTA5, and applied on Cityscapes. See details in Sec. 5.2.2.

shows an application example.

Probability simplex clustering, i.e. clustering discrete distributions, is not a new problem. It has been the subject of several early studies in the context of text analysis [12], [13], [14], among other application domains. For instance, in [15], simplex clustering is motivated for partitioning sets of text documents, and encoding them depending on their normalized word frequencies. In the context of deep learning, clustering methods have been typically used on deep feature maps, not on the outputs, as in self-training frameworks [16]. Note that the latter requires access to the internal feature maps of the source models, thereby violating the black-box assumption. Simplex-clustering based adjustment of the probabilistic outputs of a model complies with the black-box assumption, but has remained largely under-explored, to the best of our knowledge.

- F. Chiaroni is with ETS Montreal and INRS, Montreal, QC, Canada.  
E-mail: florent.chiaroni.1@etsmtl.net
- M. Boudiaf is with ETS Montreal, Montreal, QC, Canada.  
E-mail: malik.boudiaf.1@etsmtl.net
- A. Mitiche is with INRS, Montreal, QC, Canada.  
E-mail: Amar.Mitiche@inrs.ca
- I. Ben Ayed is with ETS Montreal, Montreal, Canada.  
E-mail: Ismail.BenAyed@etsmtl.ca



**Fig. 2: Modelling of softmax marginal distributions.** Figures (a), (b), (c) and (d) compare density fittings of real-world marginal distributions of softmax predictions, represented by their respective histograms (orange bars). Specifically, histograms in Fig. (a), (b), (d) were extracted from the SVHN→MNIST, and (c) from the VISDA-C softmax datasets detailed in Sec. 5.1.2. See Fig. 8 and Fig. 9 in Appendix to visualize the whole set of histograms per class. Normalized probability density functions  $\mathcal{N}$ ,  $p(\text{Eucl})$ ,  $p(\text{KL})$ ,  $p(\text{HG})$ , Beta and sBeta, are respectively obtained from the normal density, the Euclidean distance, the Kullback-Leibler divergence, the Hilbert distance, Beta, and the proposed sBeta, listed on Table. 1.

The simplex clustering literature is often based on optimizing distortion-based objectives. The goal is to minimize, within each cluster, some distortion measure evaluating the discrepancy between a cluster representative and each sample within the cluster. Besides standard objectives like K-MEANS, which correspond to an  $\|\cdot\|_2$  distortion, several simplex-clustering methods motivated and used distortion measures that are specific to simplex data. This includes, for instance, the Kullback-Leibler (KL) divergence [14], [15] and the Hilbert geometry distance [17]. In this work, we explore a general maximum a posteriori (MAP) perspective of clustering discrete distributions. Using Gibbs models, we emphasize that the density functions underlying current distortion-based objectives (Table 1) may not approximate properly the empirical marginal distributions of real-world softmax predictions (Fig. 2).

**Contributions.** Driven by the above observations, we introduce a novel probabilistic clustering objective integrating a generalization of the Beta density, which we coin sBeta. We derive several properties of sBeta, which enable to impose different constraints on our model, enforcing uni-modality of the densities within each cluster while avoiding degenerate solutions. We proceed with a block-coordinate descent approach, which alternates optimization w.r.t assignment variables and inner Newton iterations for solving the non-linear optimality conditions w.r.t the sBeta parameters. Furthermore, using the density moments, we derive a closed-form alternative to Newton iterations for parameters estimation. Our versatile formulation approximates a variety of parametric densities for modeling simplex data, including highly peaked distributions at the vertices of the simplex, as observed empirically in the case of deep-network predictions. It also enables to control the cluster balance. We report comprehensive experiments, comparisons and ablation studies, which show highly competitive performances of our simplex clustering for unsupervised adjustment of black-box predictions, in a variety of scenarios. We made available the code to reproduce our comparative experiments, including the proposed K-SBETAS model, the explored state-of-the-art approaches, as well as the introduced softmax prediction benchmarks<sup>1</sup>.

## 2 PROBLEM FORMULATION

We start by introducing the basic notations, which will be used throughout the article:

- $\Delta^{D-1} = \{\mathbf{x} \in [0, 1]^D \mid \mathbf{x}^T \mathbf{1} = 1\}$  stands for the  $(D - 1)$ -probability simplex.
- $\mathcal{X} = \{\mathbf{x}_i\}_{i=1}^N \stackrel{\text{iid}}{\sim} X$ , with  $\mathcal{X}$  a given data set and  $X$  denoting the random simplex vector in  $\Delta^{D-1}$ .
- $\mathcal{X}_k = \{\mathbf{x}_i \in \mathcal{X} \mid u_{i,k} = 1\}$  denotes cluster  $k$ , where  $\mathbf{u}_i = (u_{i,k})_{1 \leq k \leq K} \in \Delta^{K-1} \cup \{0, 1\}$  is a latent binary vector assigning point  $\mathbf{x}_i$  to cluster  $k$ :  $u_{i,k} = 1$  if  $\mathbf{x}_i$  belongs to cluster  $k$  and  $u_{i,k} = 0$  otherwise. Let  $\mathbf{U} \in \{0, 1\}^{N \times K}$  denotes the latent assignment matrix whose column vectors are given by  $\mathbf{u}_i$ . Note that  $\mathcal{X} = \mathcal{X}_1 \cup \dots \cup \mathcal{X}_{|y|}$ .

Clustering consists of partitioning a given set  $\mathcal{X}$  into  $K$  different subsets  $\mathcal{X}_k$  referred to as clusters. In general, this is done by optimizing some objective function with respect to the latent assignment variables  $\mathbf{U}$ . Often, the basic assumption underlying objective functions for clustering is that data points belonging to the same cluster  $k$  should be relatively close to each other, according to some pre-defined notion of closeness (e.g., via some distance or distortion measures).

In this study, we tackle the clustering of probability simplex data points (or distributions), with a particular focus on the output predictions from deep-learning models. Softmax<sup>2</sup> is commonly used as the last activation function of neural-network classifiers to produce such output probability distributions. Each resulting softmax data point  $\mathbf{x}$  is a  $D$ -dimensional probability vector of  $D$  continuous random variables, which are in  $[0, 1]$  and sum to one. Thus, the target clustering challenge is defined on the probability simplex domain  $\Delta^{D-1}$ . Fig. 3 illustrates this challenge with simulated mixtures of three distributions defined on  $\Delta^{(3-1)}$ . Fig. 3 (b) and (c) visually highlight the limitations of the inductive argmax prediction compared to a simplex-clustering strategy, on a simulated class-distribution shift.

2. Also referred to as the normalized exponential function, the softmax function is defined as  $\sigma(\mathbf{z})_j = \frac{\exp(z_j)}{\sum_{i=1}^D \exp(z_i)}$ , with  $\mathbf{z} = \{z_1, \dots, z_D\}$  denoting a vector of logits.

1. [https://github.com/fchiaroni/Clustering\\_Softmax\\_Predictions](https://github.com/fchiaroni/Clustering_Softmax_Predictions)

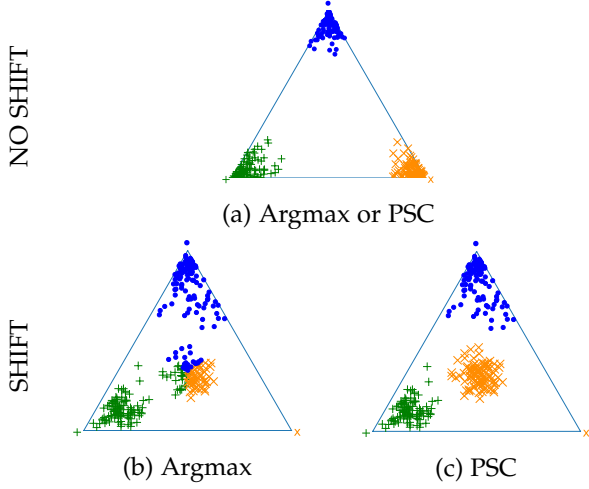


Fig. 3: Partitioning of 3-dimensional points defined on the probability simplex  $\Delta^2$ . Figures represent probability predictions from a hypothetical source model, without distribution shift in Fig. (a), and with it in Fig. (b) and (c). Fig. (b) represents the common argmax assignment. Fig. (c) represents a Probability Simplex Clustering (PSC) using cluster-to-class alignment. The symbols + (green), x (orange), • (blue) refer to separate Class assignments.

### 3 RELATED WORK

This section presents related work in the general context of clustering, with a focus on the probability simplex domain.

#### 3.1 Distortion-based clustering objectives

The most widely used form of clustering objectives is based on some *distortion* measures, for instance, a distance in general-purpose clustering or a divergence measure in the case of probability simplex data. This amounts to minimizing w.r.t both assignment variables and cluster representatives  $\Theta = (\theta_k)_{1 \leq k \leq K}$  a mixed-variable function of the following general form:

$$L_{dist}(\mathbf{U}; \Theta) = \sum_{k=1}^K \sum_{i=1}^N u_{i,k} \|\mathbf{x}_i - \theta_k\|_d = \sum_{k=1}^K \sum_{\mathbf{x}_i \in \mathcal{X}_k} \|\mathbf{x}_i - \theta_k\|_d. \quad (1)$$

The goal is to minimize, within each cluster  $\mathcal{X}_k$ , some distortion measure  $\|\cdot\|_d$  evaluating the discrepancy between cluster representative  $\theta_k$  and each point belonging to the cluster. When  $\|\cdot\|_d$  is the Euclidean distance, general form (1) becomes the standard and widely used K-MEANS objective [18]. In general, optimizing distortion-based objective (1) is NP-hard<sup>3</sup>. One standard iterative solution to tackle the problem in (1) is to follow a block-coordinate descent approach, which alternates two steps, one optimizes the objective w.r.t the cluster prototypes and the other w.r.t assignment variables:

- U-update:  $u_{i,k} = \begin{cases} 1 & \text{if } \arg \min_k \|\mathbf{x}_i - \theta_k\|_d = k \\ 0 & \text{otherwise.} \end{cases}$
- $\Theta$ -update: Find  $\arg \min_{\Theta} L_{dist}(\mathbf{U}; \Theta)$

3. For example, a proof of the NP-hardness of the standard K-MEANS objective could be found in [19].

In the specific case of K-MEANS (i.e., using the  $\|\cdot\|_2$  distance as distortion measure), optimization w.r.t the parameters in the  $\Theta$ -update step yields closed-form solutions, which correspond to the *means* of features within the clusters:

$$\theta_k = \frac{\sum_{i=1}^N u_{i,k} \mathbf{x}_i}{\sum_{i=1}^N u_{i,k}}, \forall k.$$

One way to generalize K-MEANS is to replace the Euclidean distance by other distortion measures. In this case, the optimal value of parameters  $\theta_k$  may no longer correspond to cluster means. For instance, when using the  $\|\cdot\|_1$  distance as distortion measure in (1), the optimal  $\theta_k$  corresponds to the cluster median, and the ensuing algorithm is the well-known K-MEDIAN clustering [20]. For exponential distortions, the optimal parameters may correspond to cluster modes [21], [22]. Such exponential distortions enable the model to be more robust to outliers, but this comes at the price of additional computations (inner iterations), as cluster modes could not be obtained in closed-form.

#### 3.2 Distortion measures for simplex data

In our case, data points are probability vectors within simplex domain  $\Delta^{D-1}$ , e.g. the softmax predictions of deep networks. These points are  $D$ -dimensional vectors of  $D$  continuous random variables bounded between 0 and 1, and summing to one. To our knowledge, the simplex clustering literature is often based on distortion objectives of the general form in (1). Besides standard objectives like K-MEANS, several simplex-clustering works motivated and used distortion measures that are specific to simplex data. This includes the Kullback-Leibler (KL) divergence [14], [15] and Hilbert geometry distance [17].

##### 3.2.1 Information-theoretic k-means

The works in [14], [15] discussed **KL K-MEANS**, a distortion-based clustering tailored to simplex data and whose objective fits the general form in (1). KL K-MEANS uses the Kullback-Leibler (KL) divergence as a distortion measure instead of the Euclidean distance in the standard K-MEANS:

$$\|\mathbf{x}_i - \theta_k\|_d = \text{KL}(\mathbf{x}_i \| \theta_k) = \sum_{n=1}^D x_{i,n} \log \left( \frac{x_{i,n}}{\theta_{k,n}} \right), \quad (2)$$

where  $x_{i,n}$  and  $\theta_{k,n}$  stand, respectively, for the  $n$ -th component of simplex vectors  $\mathbf{x}_i$  and  $\theta_k$ .  $\text{KL}(\mathbf{x}_i \| \theta_k)$  is a Bregman divergence [13] measuring the dissimilarity between two distributions  $\mathbf{x}_i$  and  $\theta_k$ . Despite being asymmetric [15], the KL divergence is widely used by the machine learning community, in a breadth of problems where one has to deal with probability simplex vectors [23], [24], [25], [26].

**Hilbert Simplex Clustering (HSC).** More recently, the study in [17] investigated the Hilbert Geometry (HG) distortion with *minimum enclosing ball* (MEB) centroids [27], [28] for clustering probability simplex vectors. For a given cluster set  $k$ , the MEB center represents the midpoint of the two farthest points within the set. Given two points  $\mathbf{x}_i$  and  $\theta_k$  within simplex domain  $\Delta^{D-1}$ , let  $\mathbf{x}_i + t(\theta_k - \mathbf{x}_i)$ ,  $t \in \mathbb{R}$ , denotes the line passing through points  $\mathbf{x}_i$  and  $\theta_k$ , with  $t_0 \leq 0$  and  $t_1 \geq 1$  the two intersection points of this line with

the simplex domain boundary  $\partial\Delta^{D-1}$ . Then, HG simplex distortion is given by:

$$\begin{aligned} \text{HG}_{\Delta^{D-1}}(\mathbf{x}_i; \boldsymbol{\theta}_k) &= \left| \log\left(\frac{(1-t_0)t_1}{(-t_0)(t_1-1)}\right) \right| \\ &= \log\left(1 - \frac{1}{t_0}\right) - \log\left(1 - \frac{1}{t_1}\right). \end{aligned} \quad (3)$$

Note that if one deals with centroids close or equal to the vertices of the simplex, then HG distortion would inconsistently output very large or infinite distance values at the vicinity of such centroids.

### 3.3 From distortions to probabilistic clustering

Beyond distortions, a more versatile approach is to minimize the following well-known maximum a posteriori (MAP) generalization of K-MEANS [29], [30], [31], coined by [31] as *probabilistic* K-MEANS:

$$L_{\text{prob}}(\mathbf{U}; \boldsymbol{\pi}; \boldsymbol{\Theta}) = - \sum_{k=1}^K \sum_{i=1}^N u_{i,k} \log(\pi_k f(\mathbf{x}_i; \boldsymbol{\theta}_k)), \quad (4)$$

where  $f(\cdot; \boldsymbol{\theta}_k)$  is a parametric density function modeling the likelihood probabilities of the samples within cluster  $k$ , and  $\pi_k$  the prior probability of cluster  $k$ , with  $\boldsymbol{\pi} = (\pi_k)_{1 \leq k \leq K} \in \Delta^{K-1}$ . Hence, instead of minimizing a distortion  $\|\mathbf{x}_i - \boldsymbol{\theta}_k\|_d$  in (1), we maximize a more general quantity measuring the posterior probability of cluster  $k$  given sample  $\mathbf{x}_i$  and parameters  $\boldsymbol{\theta}_k$ . It is easy to see that, for any choice of distortion measure, the objective in (1) corresponds, up to a constant, to a particular case of probabilistic K-MEANS in (4), with  $\pi_k = 1/K, \forall k$ , and parametric density  $f$  chosen to be the *Gibbs* distribution:

$$f(\mathbf{x}_i; \boldsymbol{\theta}_k) \propto \exp(-\|\mathbf{x}_i - \boldsymbol{\theta}_k\|_d). \quad (5)$$

For instance, the K-MEANS objective corresponds, up to additive and multiplicative constants, to choosing likelihood probability  $f(\mathbf{x}_i; \boldsymbol{\theta}_k)$  to be a Gaussian density with mean equal to  $\boldsymbol{\theta}_k$ , identity covariance matrix and prior probabilities verifying  $\pi_k = 1/K, \forall k$ . This uncovers hidden assumptions in K-MEANS: The samples are assumed to follow Gaussian distribution within each cluster and the clusters are assumed to be balanced<sup>4</sup>. Therefore, the general probabilistic K-MEANS formulation in (4) is more versatile as it enables to make more appropriate assumptions about the parametric statistical models of the samples within the clusters (e.g., via prior knowledge or validation data), and to manage the cluster-balance bias [29].

### 3.4 Do current simplex clustering methods model properly softmax predictions?

Eq. (5) emphasized that there are implicit density functions underlying distortion-based clustering objectives, via Gibbs models; see Table 1. Fig. 2 illustrates how the Gibbs models corresponding to the existing simplex clustering algorithms may not approximate properly the empirical marginal density functions of real-world softmax predictions:

4. In fact, it is well-known that K-MEANS has a strong bias towards balanced partitions [29]

TABLE 1: Comparison of metrics and density functions, depending on the probability simplex vector  $\mathbf{x}_i = (x_{i,n})_{1 \leq n \leq D} \in \Delta^{D-1}$  and the parameters  $\boldsymbol{\theta}_k = (\theta_{k,n})_{1 \leq n \leq D}$  for Euclidean, KL, and  $\text{HG}_{\Delta^{D-1}}$  distortions.  $\boldsymbol{\theta}_k$  respectively represents the density parameters  $\boldsymbol{\theta}_k = (\boldsymbol{\mu}_k, \Sigma_k)$  with  $\boldsymbol{\mu}_k = (\mu_{k,n})_{1 \leq n \leq D}$  for  $\mathcal{N}$ ,  $\boldsymbol{\theta}_k = (\alpha_{k,n})_{1 \leq n \leq D}$  for  $f_{\text{Dir}}$ , and  $\boldsymbol{\theta}_k = (\alpha_{k,n}, \beta_{k,n})_{1 \leq n \leq D}$  for  $g_{\text{Beta}}$  and  $g_{\text{sBeta}}$ .

METRIC-BASED	$\exp(-\text{METRIC}(\mathbf{x}_i; \boldsymbol{\theta}_k))$
$\ \mathbf{x}_i - \boldsymbol{\theta}_k\ _2$	$\exp\left(-\sqrt{\sum_{n=1}^D (x_{i,n} - \theta_{k,n})^2}\right)$
$\text{KL}(\mathbf{x}_i \  \boldsymbol{\theta}_k)$	$\prod_{n=1}^D \exp\left(-x_{i,n} \cdot \log \frac{x_{i,n}}{\theta_{k,n}}\right)$
$\text{HG}_{\Delta^{D-1}}(\mathbf{x}_i; \boldsymbol{\theta}_k)$ (EQ. (3))	$(1 - \frac{1}{t_1}) / (1 - \frac{1}{t_0})$
PROBABILISTIC	$f(\mathbf{x}_i; \boldsymbol{\theta}_k)$
$\mathcal{N}(\mathbf{x}_i; \boldsymbol{\theta}_k)$	$\frac{1}{\sqrt{(2\pi)^n  \Sigma_k }} \exp\left(-\frac{1}{2}(\mathbf{x}_i - \boldsymbol{\mu}_k)^T \Sigma_k^{-1} (\mathbf{x}_i - \boldsymbol{\mu}_k)\right)$
$f_{\text{Dir}}(\mathbf{x}_i; \boldsymbol{\theta}_k)$	$\frac{\prod_{n=1}^D x_{i,n}^{(\alpha_{k,n}-1)}}{B(\boldsymbol{\theta}_k)}$
$g_{\text{Beta}}(\mathbf{x}_i; \boldsymbol{\theta}_k)$	$\prod_{n=1}^D \frac{(x_{i,n})^{\alpha_{k,n}-1} (1-x_{i,n})^{\beta_{k,n}-1}}{B(\alpha_{k,n}, \beta_{k,n})}$
$g_{\text{sBeta}}(\mathbf{x}_i; \boldsymbol{\theta}_k)$	$\prod_{n=1}^D \frac{(x_{i,n} + \delta)^{\alpha_{k,n}-1} (1 + \delta - x_{i,n})^{\beta_{k,n}-1}}{B(\alpha_{k,n}, \beta_{k,n})(1 + 2\delta)^{\alpha_{k,n} + \beta_{k,n} - 2}}$

**Standard K-MEANS: Fast, but not descriptive enough and biased.** The well-known K-MEANS clustering falls under the probabilistic clustering framework, as defined in Sec. 3.3. In particular, it instantiates the data likelihoods as Gaussian densities with unit covariance matrices. An important advantage of K-MEANS is that the associated  $\boldsymbol{\Theta}$ -update step can be analytically solved by simply updating each  $\boldsymbol{\theta}_k$  as the mean of samples within cluster  $k$ , according to the current latent assignments. Such closed-form solutions enable K-MEANS to be among the most efficient clustering algorithms. However, the Gaussian assumption yielding such closed-form solutions might be limiting when dealing with asymmetric data densities such as exponential densities, with the particularity that the mode and the mean are distinct. As depicted by Fig. 2 (a) and (b), the softmax outputs from actual deep-learning models commonly follow such asymmetric distributions. Note that K-MEANS and other distortion-based objectives correspond to setting  $\pi_k = 1/K, \forall k$  in the general probabilistic formulation in Eq. (4). Therefore, they encode the implicit strong bias towards balanced partitions [29], and might be sub-optimal when dealing with imbalanced clusters, as is often the case of realistic deep-network predictions.

**Elliptic K-MEANS.** Elliptic K-MEANS is a generalization of the standard K-means: It uses the Mahalanobis distance instead of the Euclidean distance, which assumes the data within each cluster follows a Gaussian distribution (i.e. Gibbs model for the Mahalanobis distance) whose covariance matrix is also a variable of the model (as opposed to unit covariance in K-MEANS); see Table 1. Fig. 2 (b) and (c) confirm that Gaussian density function  $\mathcal{N}$  is not appropriate for



skewed distributions, as is the case of network predictions.

**HSC yields poor approximations of highly peaked distributions located at the vertices of the simplex.** Fig. 2 shows that HSC, which combines MEB centroids and HG metric, is not relevant to asymmetric distributions whose modes are close to the vertices of the simplex. Specifically, in Fig. 2 (a) and (b), the corresponding Gibbs probability is small near the vertices of the simplex and high at the middle of the simplex. This yields poor approximation of the target empirical histograms (depicted in orange). In addition, the overall HSC algorithm is computationally demanding (see Table. 3).

**KL K-MEANS.** While KL could yield asymmetric density, it may poorly model highly peaked distributions at the vertices of the simplex (e.g. Fig. 2 a), as is the case of softmax predictions.

## 4 PROPOSED APPROACH

### 4.1 Background

#### Dirichlet density function.

Multivariate Dirichlet densities are commonly used in Bayesian statistics for modeling categorical events. The domain of the Dirichlet density is the set of  $D$ -dimensional discrete distributions, i.e. the set of vectors within  $(D - 1)$ -simplex  $\Delta^{D-1}$ . The Dirichlet density with parameter vector  $\alpha = (\alpha_n)_{1 \leq n \leq D} \in \mathbb{R}^D$  has the following expression:

$$f_{\text{Dir}}(\mathbf{x}; \alpha) = \frac{1}{B(\alpha)} \prod_{n=1}^D x_n^{\alpha_n-1}, \quad (6)$$

for  $\mathbf{x} \in \Delta^{D-1}$ .  $B$  denotes the multivariate Beta function, which could be expressed with the Gamma function<sup>5</sup>:

$$B(\alpha) = \frac{\prod_{n=1}^D \Gamma(\alpha_n)}{\Gamma(\sum_{n=1}^D \alpha_n)}.$$

One could envision to use the Dirichlet density along with the probabilistic K-MEANS objective in (4), to deal with simplex data such as softmax predictions. While Dirichlet is specifically designed to model simplex vectors, to the best of our knowledge, it is not commonly used in simplex clustering, which may seem surprising. This might be explained by the fact that the Dirichlet density is highly descriptive, e.g. it allows multi-modal representations of the samples within each cluster. Therefore, using it in general probabilistic clustering objective (4) results in challenging, computationally heavy optimization problems. First, a block-coordinate descent alternating Dirichlet-parameter estimation and cluster assignments may get stuck into weak local minima. Secondly, it is well-known that the estimation of Dirichlet parameters from a fixed set of samples is computationally demanding [32], requiring fixed-point and Newton-Raphson iterations. In clustering, such cumbersome estimation has to be performed as inner iterations, after each outer iteration of clustering update, resulting in computationally heavy procedures.

As an efficient alternative, we propose to use the mean-field approximation principle [33], which is widely used in variational inference and graphical models, to formulate a relaxed product density form of Dirichlet. This factorisation

depends on its marginal Beta density function with  $\alpha$  and  $\beta$  parameters, and is defined as:

$$\begin{aligned} g_{\text{Beta}}(\mathbf{x}; \alpha, \beta) &= \prod_{n=1}^D f_{\text{Beta}}(x_n; \alpha_n, \beta_n) \\ &= \prod_{n=1}^D \frac{(x_n)^{\alpha_n-1} (1-x_n)^{\beta_n-1}}{B(\alpha_n, \beta_n)} \\ &\approx f_{\text{Dir}}(\mathbf{x}; \alpha), \end{aligned} \quad (7)$$

with  $B(\alpha, \beta) = \frac{\Gamma(\alpha)\Gamma(\beta)}{\Gamma(\alpha+\beta)}$ . This joint density function  $g_{\text{Beta}}$  assumes that each simplex coordinate is independent of the other coordinates. This enables to estimate independently the parameters of each marginal Beta using density moments, which drastically reduces the computational burden.

Apart from computational load, we discuss in the following how Dir and Beta may yield poor approximations of the empirical marginal density functions of real-world softmax predictions (Fig. 2), which motivates our introduced sBeta density.

#### Do Dir and Beta model properly softmax predictions?

Fig. 2 shows how Beta may yield poor approximations of the empirical marginal density functions of real-world softmax predictions near the vertices of the simplex:

- Fig. 2 (a) and (b) show how marginal probability Beta has difficulty capturing highly peaked empirical density functions near the vertices of the simplex (i.e. near values 0 and 1), unlike the proposed sBeta.
- Dir allows multimodal distributions, as shown with its Beta marginal in Fig. 2 (d). Indeed, when the estimated parameters verify  $0 < \alpha_1, \dots, \alpha_D < 1$ , the resulting Dir could have multiple modes at the vertices of the simplex; see the density depicted in red color in Fig. 4 (a). The main risk with this property is that a Dir-based clustering may model  $K$  separate unimodal distributions as a unique multimodal distribution. However in our targeted scenario, we commonly assume that each semantic class is represented by a unimodal distribution because of the following reason: Discriminative deep learning models are optimized to output probability simplex vertices (i.e. one-hot vectors). Hence, for each class, the model is optimized to generate softmax predictions following a separate unimodal distribution. In this context, Dir may erroneously model two of such distributions as a single bimodal distribution.

In the next section, we propose an alternative of Dir and Beta, which can deal with the two limitations discussed above.

### 4.2 Proposed density function: A generalization of Beta constrained to be unimodal

Unlike Beta, we want a density function that enables to approximate highly peaked densities at the vertices of the simplex, while satisfying a uni-modality constraint, thereby avoiding degenerate solutions and accounting for the statistical properties of real-world softmax predictions.

5. The Gamma function is given by:  $\Gamma(\alpha) = \int_0^\infty t^{\alpha-1} \exp(-t) dt$  for  $\alpha > 0$ . Note that  $\Gamma(\alpha) = (\alpha - 1)!$  when  $\alpha$  is a strictly positive integer.

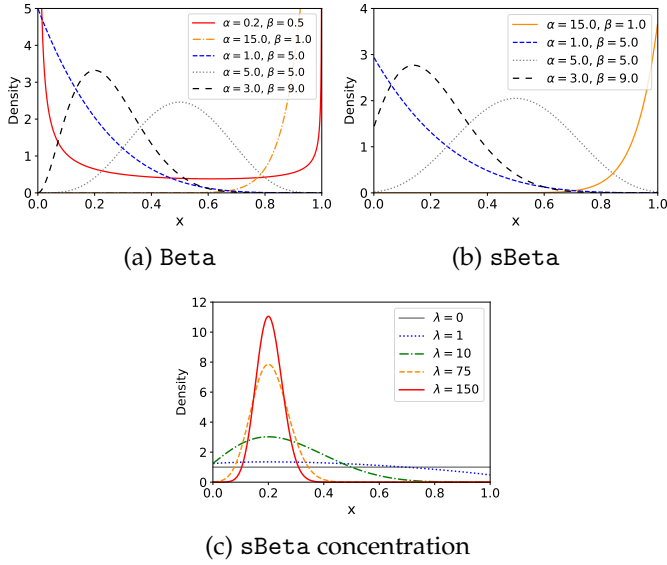


Fig. 4: **Beta and sBeta density functions.** Figures (a) and (b) respectively illustrate Beta density function, and the presented variant referred to as sBeta. Fig. (c) shows sBeta depending on the concentration parameter  $\lambda$  while maintaining the same mode.

#### 4.2.1 Generalization of Beta

We propose the following generalization of Beta, which we refer to as sBeta (scaled Beta) in the sequel:

$$f_{\text{sBeta}}(x; \alpha, \beta) = \frac{(x + \delta)^{\alpha-1} (1 + \delta - x)^{\beta-1}}{B(\alpha, \beta) (1 + 2\delta)^{\alpha+\beta-2}}, \quad (8)$$

with  $\delta \in \mathbb{R}^+$ . Clearly, when parameter  $\delta$  is set equal to 0, the generalization in (8) reduces to Beta density  $f_{\text{Beta}}$  in (7). Figures 4 (a) and (b) depict Beta and sBeta density functions for different values of parameters  $\alpha$  and  $\beta$ , showing the difference between the two densities. For instance, for  $\alpha = 3$  and  $\beta = 9$ , one may observe that sBeta yields a density mode closer to the simplex vertex (which corresponds to value 0 in this particular example). Therefore, as illustrated in Figs. 2 (a), (b) and (c), this yields approximations of the empirical distributions (orange histograms) of the softmax predictions that are better than those obtained with the Beta density. Overall, sBeta could be viewed as a scaled variant of Beta, which is relatively more permissive, fitting a wider range of uni-modal simplex distributions.

In the following, we provide expressions of the moments (first and second central) and mode of sBeta as functions of density parameters  $\alpha$  and  $\beta$ . As we will see shortly, these properties will enable us to integrate different constraints with our sBeta-based probabilistic clustering objective, enforcing uni-modality of the distribution within each cluster while avoiding degenerate solutions. Furthermore, they will enable us to derive a computationally efficient, moment-based estimation of the densities parameters.

#### 4.2.2 Mean and Variance

**Property 1.** The mean  $E_{\text{sBeta}}[X]$  of sBeta could be expressed as a function of the density parameters as follows:

$$E_{\text{sBeta}}[X] = \frac{\alpha}{\alpha + \beta} (1 + 2\delta) - \delta. \quad (9)$$

*Proof.* The mean  $E_{\text{sBeta}}[X]$  of sBeta could be found by integrating  $x f_{\text{sBeta}}(x)$ . A detailed derivation is provided in Appendix A.  $\square$

**Property 2.** The variance  $V_{\text{sBeta}}[X]$  of sBeta could be expressed as a function of the density parameters as follows:

$$V_{\text{sBeta}}[X] = \frac{\alpha\beta}{(\alpha + \beta)^2(\alpha + \beta + 1)} (1 + 2\delta)^2. \quad (10)$$

*Proof.* We use  $V_{\text{sBeta}}[X] = E_{\text{sBeta}}[X^2] - E_{\text{sBeta}}[X]^2$ , with  $E_{\text{sBeta}}[X^2]$  denoting the second moment of sBeta, which could be found by integrating  $x^2 f_{\text{sBeta}}(x)$ . The details of the computations of  $E_{\text{sBeta}}[X^2]$  and  $V_{\text{sBeta}}[X]$  are provided in Appendix. A.  $\square$

#### 4.2.3 Mode and Concentration

The mode of a density function  $f(x)$  corresponds to the value of  $x$  at which  $f(x)$  achieves its maximum.

**Property 3.** The mode  $m_{\text{sBeta}}$  of sBeta could be expressed as a function of the density parameters as follows:

$$m_{\text{sBeta}} = \frac{\alpha - 1 + \delta(\alpha - \beta)}{\alpha + \beta - 2}. \quad (11)$$

*Proof.* The mode  $m_{\text{sBeta}}$  of sBeta can be found by estimating at which value of  $x$  the derivative of  $f_{\text{sBeta}}$  is equal to 0. A detailed derivation could be found in Appendix A.  $\square$

Note that, when  $\alpha = \beta$ , we have  $m_{\text{sBeta}} = E_{\text{sBeta}}[X] = \frac{1}{2}$ . Otherwise,  $m_{\text{sBeta}} \neq E_{\text{sBeta}}[X]$ . Thus, sBeta is asymmetric when  $\alpha \neq \beta$  and the variance is consequently not adequate to measure the dispersion around sBeta mode.

**Concentration parameter.** Motivated by the previous observation, we present the concentration parameter  $\lambda$  to measure how much a sample set is condensed around the mode value. The concept of concentration parameter has been previously discussed in [34]. With respect to the mode equation 11, we express  $\lambda = \alpha + \beta - 2$  such that we have

$$m_{\text{sBeta}} = \frac{\alpha - 1 + \delta(\alpha - \beta)}{\lambda}. \quad (12)$$

Using Eq. (12), we can express  $\alpha$  and  $\beta$  as functions of the mode and concentration parameter:

$$\begin{cases} \alpha = 1 + \lambda \frac{m_{\text{sBeta}} + \delta}{1 + 2\delta} \\ \beta = 1 + \lambda \frac{1 + \delta - m_{\text{sBeta}}}{1 + 2\delta} \end{cases} \quad (13)$$

Fig. 4 (c) shows different concentrations around a given mode when changing  $\lambda$ .

### 4.3 Proposed clustering model: K-SBETAS

**Probabilistic clustering.** We cast clustering distributions as minimizing the following probabilistic objective (K-SBETAS), which measures the conformity of data within each cluster to a multi-variate sBeta density function, subject to constraints that enforce uni-modality and discourage degenerate solutions:

$$L_{\text{sBeta}}(\mathbf{U}; \boldsymbol{\pi}; \boldsymbol{\Theta}) = - \sum_{i=1}^N \sum_{k=1}^K u_{i,k} \log(\pi_k g_{\text{sBeta}}(\mathbf{x}_i; \boldsymbol{\alpha}_k, \boldsymbol{\beta}_k)) \quad (14)$$

$$\text{s.t. } \begin{cases} \lambda_{k,n} \geq \tau^- \forall k, n : \text{Unimodal constraint, Sec. 4.3.2} \\ \lambda_{k,n} \leq \tau^+ \forall k, n : \text{Avoids Dirac solutions, Sec. 4.3.2} \end{cases} \quad (15)$$

where  $g_{\text{sBeta}}$  is a multivariate extension of sBeta:

$$g_{\text{sBeta}}(\mathbf{x}_i; \boldsymbol{\alpha}_k, \boldsymbol{\beta}_k) = \prod_{n=1}^D f_{\text{sBeta}}(x_{i,n}; \alpha_{k,n}, \beta_{k,n}),$$

and  $\lambda_{k,n}$  denotes the concentration parameter of univariate  $f_{\text{sBeta}}(x_{i,n}; \alpha_{k,n}, \beta_{k,n})$ . In our model in (14),  $\Theta = (\boldsymbol{\alpha}_k, \boldsymbol{\beta}_k)_{1 \leq k \leq K}$ , with  $\boldsymbol{\alpha}_k = (\alpha_{k,n})_{1 \leq n \leq D}$  and  $\boldsymbol{\beta}_k = (\beta_{k,n})_{1 \leq n \leq D}$ ,  $\boldsymbol{\pi} = (\pi_k)_{1 \leq k \leq K} \in \Delta^{K-1}$  and, following the general notation we introduced in Sec. 2,  $\mathbf{U}$  denotes binary point-to-cluster assignments.

#### 4.3.1 Block-coordinate descent optimization

Our objective in (14) depends on three different sets of variables:  $\mathbf{U}$ ;  $\boldsymbol{\pi}$ ; and sBeta parameters  $\Theta$ . Therefore, we proceed with a block-coordinate descent approach, which alternates three steps. Each step optimizes the objective w.r.t a set of variables while keeping the rest of the variables fixed.

- **$\Theta$  updates, with  $\mathbf{U}$  and  $\boldsymbol{\pi}$  fixed:** This section presents two different strategies for updating the sBeta parameters:

(a) *Solving the necessary conditions for the minimum of  $L_{\text{sBeta}}$  w.r.t  $\alpha_{k,n}$  and  $\beta_{k,n}$ :*

Our objective in (14) is convex in each  $\alpha_{k,n}$  and  $\beta_{k,n}$ . The global optima could be obtained by setting the gradient to zero. This could be viewed as a maximum likelihood estimation approach (MLE). Unfortunately, this yields a non-linear system of equations that, cannot be solved in closed-form. Therefore, we proceed to an inner iteration. In the appendix, we derive the following iterative and alternating updates to solve the non-linear system of equations:

$$\begin{aligned} \alpha_k^{(t+1)} &= \psi^{-1}(\psi(\alpha_k^{(t)} + \beta_k^{(t)}) \\ &\quad + \frac{1}{\sum_{i=1}^N u_{i,k}} \sum_{i=1}^N u_{i,k} \log(\frac{\mathbf{x}_i + \delta}{1 + 2\delta})) \quad (16) \\ \beta_k^{(t+1)} &= \psi^{-1}(\psi(\alpha_k^{(t)} + \beta_k^{(t)}) \\ &\quad + \frac{1}{\sum_{i=1}^N u_{i,k}} \sum_{i=1}^N u_{i,k} \log(\frac{1 + \delta - \mathbf{x}_i}{1 + 2\delta})) \quad (17) \end{aligned}$$

where  $t$  refers to iteration number and  $\psi$  corresponds to the digamma function. Note that neither  $\psi$  nor  $\psi^{-1}$  admit analytic expressions. Instead, we follow [32] to approximate those functions, at the cost of additional Newton iterations. The full derivation of the updates and all required details could be found in the Appendix.

(b) *Method of moments (MoM):*

As a computationally efficient alternative to solving a non-linear system within each outer iteration, we introduce an approximate estimation of sBeta parameters  $\boldsymbol{\alpha}_k$  and  $\boldsymbol{\beta}_k$ , which we denote  $\hat{\boldsymbol{\alpha}}_k$  and  $\hat{\boldsymbol{\beta}}_k$ , as

the solutions to the first and second central moment equations, following Prop. 1 and Prop. 2:

$$\begin{cases} \boldsymbol{\mu}_k &= \frac{\boldsymbol{\alpha}_k}{\boldsymbol{\alpha}_k + \boldsymbol{\beta}_k} (1 + 2\delta) - \delta \\ \mathbf{v}_k &= \frac{\boldsymbol{\alpha}_k \boldsymbol{\beta}_k}{(\boldsymbol{\alpha}_k + \boldsymbol{\beta}_k)^2 (\boldsymbol{\alpha}_k + \boldsymbol{\beta}_k + 1)} (1 + 2\delta)^2 \end{cases} \quad (18)$$

where  $\boldsymbol{\mu}_k$  and  $\mathbf{v}_k$  denote, respectively, the empirical means and variances of cluster  $k$ :

$$\boldsymbol{\mu}_k = \frac{\sum_{i=1}^N u_{i,k} \mathbf{x}_i}{\sum_{i=1}^N u_{i,k}} \text{ and } \mathbf{v}_k = \frac{\sum_{i=1}^N u_{i,k} (\mathbf{x}_i - \boldsymbol{\mu}_k)^2}{\sum_{i=1}^N u_{i,k}}. \quad (19)$$

The system of two equations and two unknowns in (18) could be solved efficiently in closed-form, which yields the following estimates of sBeta parameters:

$$\begin{cases} \alpha_k &= (\frac{\boldsymbol{\mu}_k^\delta (1 - \boldsymbol{\mu}_k^\delta) (1 + 2\delta)^2}{\mathbf{v}_k} - 1) \boldsymbol{\mu}_k^\delta \\ \beta_k &= (\frac{\boldsymbol{\mu}_k^\delta (1 - \boldsymbol{\mu}_k^\delta) (1 + 2\delta)^2}{\mathbf{v}_k} - 1) (1 - \boldsymbol{\mu}_k^\delta) \end{cases} \quad (20)$$

with  $\boldsymbol{\mu}_k^\delta = \frac{\boldsymbol{\mu}_k + \delta}{1 + 2\delta}$ .

- **$\mathbf{U}$  updates, with  $\Theta$  and  $\boldsymbol{\pi}$  fixed:** With variables  $\Theta$  and  $\boldsymbol{\pi}$  fixed, the global optimum of our objective in (14) with respect to assignment variables  $\mathbf{U}$ , subject to constraints  $\mathbf{u}_i = (u_{i,k})_{1 \leq k \leq K} \in \Delta^{K-1} \cup \{0, 1\}$ , corresponds to the following closed-form solution for each assignment variable  $u_{i,k}$ :

$$u_{i,k} = \begin{cases} 1 & \text{if } \arg \max_k \pi_k \cdot g_{\text{sBeta}}(\mathbf{x}_i; \boldsymbol{\alpha}_k, \boldsymbol{\beta}_k) = k \\ 0 & \text{otherwise.} \end{cases} \quad (21)$$

- **$\boldsymbol{\pi}$  updates, with  $\mathbf{U}$  and  $\Theta$  fixed:** Solving the Karush–Kuhn–Tucker (KKT) conditions for the minimum of (14) with respect to  $\boldsymbol{\pi}$ , s.t  $\boldsymbol{\pi} \in \Delta^{K-1}$ , yields the following closed-form solution for each  $\pi_k$ :

$$\pi_k = \frac{\sum_{i=1}^N u_{i,k}}{N}. \quad (22)$$

#### 4.3.2 Handling parameters constraints

Our model in (14) integrates two constraints on concentration parameters  $\lambda_{k,n}$ , one discourages multi-modal solutions and the other avoids degenerate, highly peaked (Dirac) densities.

Notice that the sBeta density is bimodal when  $\alpha_{k,n} < 1$  and  $\beta_{k,n} < 1$ , which corresponds to  $\lambda_{k,n} < 0$  (as  $\lambda_{k,n} = \alpha_{k,n} + \beta_{k,n} - 2$ ). Moreover, setting  $\alpha_{k,n} = \beta_{k,n} = 1$ , which yields  $\lambda_{k,n} = 0$ , corresponds to the uniform density. Thus, to constrain the sBeta densities to be strictly unimodal, we have to restrict  $\lambda_{k,n}$  to positive values. In practice, we constrain  $\lambda_{k,n}$  to be greater or equal than a threshold  $\tau^- > 0$ , which we simply set to 1.

A high density concentration around the sBeta mode corresponds to high values  $\lambda_{k,n}$ . Thus, to avoid degenerate, highly peaked (Dirac) densities, we constrain  $\lambda_{k,n}$  to stay smaller or equal than a fixed, strictly positive threshold  $\tau^+$ .

Overall, we enforce  $\tau^- \leq \lambda_{k,n} \leq \tau^+$  on sBeta parameters using Eq. (13), as detailed in Algorithm 1. This procedure enables to maintain the same density mode. Fig. 5 (a) shows sBeta density estimation, following the constraint  $\lambda_{k,n} \geq \tau^-$ , on a bimodal distribution sample. Fig. 5 (b) shows sBeta estimation, following the constraint  $\lambda_{k,n} \leq \tau^+$ , on a Dirac distribution sample.

---

**Algorithm 1** Constraints for sBeta parameters
 

---

```

1: global variables
2:    $\delta$ , the sBeta hyper-parameter
3:    $\tau^-$ , the unimodal constraint
4:    $\tau^+$ , the constraint to avoid Dirac solutions
5: end global variables
6: function CONSTRAIN( $\alpha_k, \beta_k$ )
7:    $m_{sB} \leftarrow \frac{\alpha_k - 1 + \delta(\alpha_k - \beta_k)}{\alpha_k + \beta_k - 2}$   $\triangleright$  Estimate the mode
8:    $\lambda_k \leftarrow \alpha_k + \beta_k - 2$   $\triangleright$  Estimate the concentration
9:   for  $n \leftarrow 1 \dots D$  do
10:    if  $\lambda_{k,n} < \tau^-$  then
11:       $\lambda_{k,n} \leftarrow \tau^-$   $\triangleright$  Ensure strictly unimodal
    solutions
12:    else if  $\lambda_{k,n} > \tau^+$  then
13:       $\lambda_{k,n} \leftarrow \tau^+$   $\triangleright$  Avoid Dirac solutions
14:    end if
15:  end for
16:   $\alpha_k \leftarrow 1 + \lambda_k \frac{m_{sB} + \delta}{1 + 2\delta}$   $\triangleright$  Update  $\alpha_k$  using (13)
17:   $\beta_k \leftarrow 1 + \lambda_k \frac{1 + \delta - m_{sB}}{1 + 2\delta}$   $\triangleright$  Update  $\beta_k$  using (13)
18:  return  $\alpha_k, \beta_k$ 
19: end function
  
```

---

#### 4.3.3 Centroids initialization

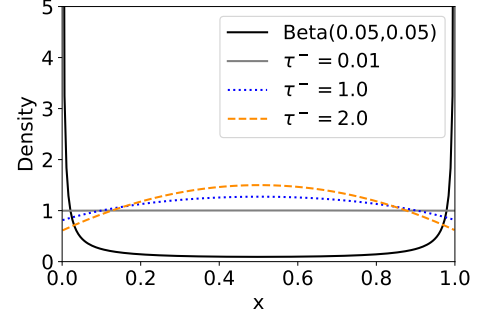
Clustering algorithms are known to be sensitive to their parameters initialization. They often converge to a local optimum. To reduce this limitation, the seeding initialization strategy k-means++, proposed in [35] and then thoroughly studied in [36], is broadly used for centroids initialization. However, in the context of the clustering of softmax predictions, we can assume that softmax predictions generated by deep learning models were optimized in upstream to be sets of one-hot vectors<sup>6</sup>. Thus, we propose to initialize the centroids as vertices of the target probability simplex domain. More specifically, we initialize all  $\alpha_{k,n}$  and  $\beta_{k,n}$  parameters such that they model exponential densities on  $[0, 1]$  at the start. In other words, each initial mode is set as a vertex among all possible vertices on the probability simplex domain. Beyond improving K-SBETAS, this simple initialization strategy unanimously improves the scores of every tested clustering method<sup>7</sup>.

#### 4.3.4 From cluster-labels to class-labels assignment

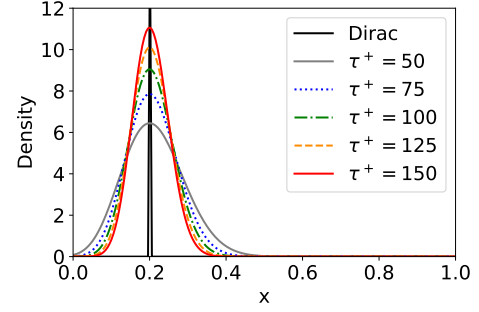
Downstream to the clustering process, we have to align cluster-labels with target class-labels. One can align each cluster centroid with the closest one-hot vector by using the argmax function. However, if a one-hot vector referring to a given class is the closest vertex for several cluster centroids, then several cluster sets would be assigned with the same class. To prevent this problem on closed-set challenges, i.e. with the prior knowledge  $K = D$ , we use the optimal transport Hungarian algorithm [37]. Specifically, we compute the Euclidean distances between all centroids and one-hot vectors. Then, we apply the Hungarian algorithm on this matrix of distances to find the lowest-cost way to assign a separate class to each cluster.

6. A one-hot vector both refers to a semantic class and to a vertex on the probability simplex.

7. Table 12 in Appendix empirically supports this statement.



(a) Avoid bimodal solutions



(b) Avoid Dirac solutions

Fig. 5: Visualization of the introduced constraints. Fig. (a) shows sBeta density estimation, constrained with the threshold  $\tau^-$ , on a sample following a bimodal Beta distribution. Fig. (b) shows sBeta density estimation, constrained with the threshold  $\tau^+$ , on a sample following a Dirac distribution.

## 5 EXPERIMENTS

Throughout this section, we empirically compare the proposed method with state-of-the-art clustering methods previously discussed in Sec. 3. We first validate our implementations on synthetic datasets and on softmax predictions from unsupervised domain adaptation (UDA) source models. We further showcase the usefulness across the two real-world tasks One-Shot learning and UDA road segmentation, in which our method is used as a plug-in on top of output predictions from a black-box deep learning model. We also highlight the effect of each component of the proposed framework along ablation studies.

**Compared methods.** We compare several state-of-the-art clustering methods. Specifically, comparative experiments include KL K-MEANS [15] [14] and HSC [17], two methods that are specifically designed to deal with probability simplex vectors. We additionally compare in this study generic clustering methods K-MEANS, GMM [38], K-MEDIANS [20], K-MEDOIDS [39], K-MODES [21]. Both K-MEANS and KL K-MEANS use mean centroids, but respectively euclidean and Kullback-Leibler distortions. K-MEDIANS, extensively studied in [20], uses median centroids and the Manhattan distance. K-MEDOIDS uses the euclidean distance and it estimates its medoid centroids with the standard PAM algorithm [39]. K-MODES [21] uses euclidean distance as well, and its mode centroids are estimated using the Meanshift algorithm [40] with the window size 0.05.

**K-DIRS.** We also implemented a simplex clustering strategy consisting of estimating multivariate densities per



---

**Algorithm 2** k-sBetas algorithm.

---

**Input:** Dataset of probability simplex points defined as  $\mathcal{X} = \{\mathbf{x}_i\}_{i=1}^N \in \Delta^{D-1}$ , with  $N$  the total number of points. Number of clusters  $K$ . The maximum number  $t_{end}$  of iterations.

**Output:**  $\mathbf{U}$ , the clustering hard labels assignments

```

1: global variables
2:    $\delta$ , the sBeta hyper-parameter
3:    $\tau^-$ , the unimodal constraint
4:    $\tau^+$ , the constraint to avoid Dirac solutions
5: end global variables
6:  $\mathbf{U} \leftarrow [0]_{N,K}$   $\triangleright$  Arbitrary labels initialization
7:  $\boldsymbol{\pi} \leftarrow \{\frac{1}{K}\}_{k=1}^K$   $\triangleright$  Initialize uniform class proportions
8: Initialize  $\Theta$  using vertices init  $\triangleright$  Sec. 4.3.3.
9:  $t \leftarrow 0$ 
10: repeat
11:   if  $t > 0$  then
12:     for  $k \leftarrow 1 \dots K$  do  $\triangleright$  Loop over clusters
13:       Estimate  $\boldsymbol{\alpha}_k, \boldsymbol{\beta}_k$  with MoM/MLE  $\triangleright$  Sec. 4.3.1.
14:        $\boldsymbol{\alpha}_k, \boldsymbol{\beta}_k \leftarrow \text{CONSTRAIN}(\boldsymbol{\alpha}_k, \boldsymbol{\beta}_k)$   $\triangleright$  Algorithm 1
15:     end for
16:   end if
17:   for  $i \leftarrow 1 \dots N$  do  $\triangleright$  hard label assignment
18:     for  $k \leftarrow 1 \dots K$  do
19:       if  $\arg \max_k \pi_k \cdot g_{\text{sBeta}}(\mathbf{x}_i; \boldsymbol{\alpha}_k, \boldsymbol{\beta}_k) = k$  then
20:          $u_{i,k} \leftarrow 1$ 
21:       else
22:          $u_{i,k} \leftarrow 0$ 
23:       end if
24:     end for
25:   end for
26:    $\boldsymbol{\pi} \leftarrow \frac{\sum_{i=1}^N \mathbf{u}_i}{N}$   $\triangleright$  Estimate class proportions
27:    $t \leftarrow t + 1$ 
28: until convergence or  $t = t_{end}$ 
29: return  $\mathbf{U}$ 

```

---

cluster with Dirichlet density function. We use the iterative parameters estimation previously proposed in [32]. This algorithm, referred to as K-DIRS, represents a baseline on the artificial datasets composed of Dirichlet distributions.

**Proposed K-SBETAS.** Our clustering algorithm uses the density function  $f_{\text{sBeta}}$  and the method of moments (MoM) detailed in Sec. 4.3.1 for parameters estimation. We empirically consolidate this choice in the ablation study section 5.3. K-BETAS corresponds to the un-scaled variant of K-SBETAS when we set  $\delta = 0$ .

**Details and hyper-parameters.** Across all experiments, we set the scaling hyper-parameter  $\delta$  used in K-SBETAS to the same value 0.15. We set  $\tau^- = 1$  and  $\tau^+ = 165$  for parameters constraints. The maximum number of clustering iterations is set to 25 for all compared clustering algorithms. Finally, for each method, we use the proposed vertices parameters initialization, and leverage the Hungarian algorithm to obtain optimal hard-label assignments. We provide comparisons and justifications for our design choices in the ablation studies in Sec. 5.3.

**Methods reproducibility.** We use scikit-learn library

implementation for GMM<sup>8</sup>, and the authors implementation for HSC<sup>9</sup>. We have implemented all the other clustering algorithms<sup>10</sup>.

**Evaluation metrics.** We use the standard *Normalized Mutual Information* (NMI) on each dataset to evaluate the clustering task, and the classification *Accuracy* (Acc) or *Intersection over Union* (IoU) respectively on balanced and imbalanced datasets to evaluate prediction scores for the class assignment task.

## 5.1 Comparative experiments

### 5.1.1 Synthetic experiments

The purpose of synthetic experiments is to benchmark clustering methods on a simple, artificially generated task.

**Simu dataset.** We aim to generate balanced mixtures composed of three Dirichlet distributions, defined on the 3-dimensional probability simplex  $\Delta^2$ . Respective Dirichlet density parameters are  $\boldsymbol{\alpha}_1 = (1, 1, 5)$ ,  $\boldsymbol{\alpha}_2 = (25, 5, 5)$ ,  $\boldsymbol{\alpha}_3 = (5, 7, 5)$ . Each component is purposefully biased towards one different vertex of the simplex, and can be intuitively thought as representing the softmax predictions of a deep learning model for a certain class. Additionally, each component captures a different type of distribution<sup>11</sup>:  $\text{Dir}(\boldsymbol{\alpha}_1)$  represents an exponential distribution on  $\Delta^2$ ,  $\text{Dir}(\boldsymbol{\alpha}_2)$  represents an off-centered distribution having a small variance, while the latter represents a relatively more centered one, with a wider variance and similar to a Gaussian distribution. All components equally contribute to the final mixture. In total, 100 000 examples are sampled. We perform 5 random runs, each using new examples.

**Results.** Table 2 shows NMI and Acc scores of compared approaches on the proposed Simu dataset. As expected, Table 2 shows close scores for K-DIRS and K-BETAS as they both model Beta marginal densities. K-SBETAS naturally provides lower scores due to the scaling factor  $\delta > 0$ , while showing more adequacy than the state-of-the-art.

### 5.1.2 Softmax predictions from deep learning models

We now compare approaches on real-world mixtures of distributions, where points to cluster correspond to softmax predictions from actual deep learning models.

**Setup.** First, we employ the **SVHN**→**MNIST** challenge, where a source model is trained on SVHN [41] and applied on MNIST [42] test set, composed of 10 000 images labelled with 10 different semantic classes. Additionally, we experiment with the more difficult **VISDA-C** challenge [43], which contains 55 388 examples across 12 different semantic classes. Respectively for **SVHN**→**MNIST** and **VISDA-C**, we follow the common network architectures and training

8. GMM code is available at: [https://github.com/scikit-learn/scikit-learn/blob/7e1e6d09b/sklearn/mixture/\\_gaussian\\_mixture.py](https://github.com/scikit-learn/scikit-learn/blob/7e1e6d09b/sklearn/mixture/_gaussian_mixture.py)

9. HSC code is available at: <https://franknielsen.github.io/HSG/>.

10. KL K-MEANS, K-MEANS, K-MEDIANS, K-MEDIODS, K-MODES, K-DIRS, K-BETAS and K-SBETAS codes are available at: [https://github.com/fchiaroni/Clustering\\_Softmax\\_Predictions](https://github.com/fchiaroni/Clustering_Softmax_Predictions)

11. We provide the 2D visualizations of these simulated distributions in Appendix, Fig. 7.

TABLE 2: Comparative **probability simplex clustering** on *Simu*, SVHN→MNIST and VISDA-C datasets. The FEATURE MAP layer is the bottleneck layer on top of the convolutional layers. It outputs a feature vector of size 256 for each input image. The LOGITS points are obtained with the fully connected classifier on top of the bottleneck layer, so that the logit point predicted for each input example is a vector of size  $K$ . The probability SIMPLEX points, which represent the predictions of a black-box model, are obtained with the standard softmax function on top of the LOGITS layer.

METHOD	LAYER USED	SIMU	SVHN→MNIST		VISDA-C	
		(NMI)	(NMI)	(ACC)	(NMI)	(ACC)
K-MEANS	FEATURE MAP	-	67.3	74.3	30.0	22.7
K-MEANS	LOGITS	-	67.1	74.5	32.7	33.1
ARGMAX	SIMPLEX (BLACK-BOX)	60.1	58.6	69.8	36.5	53.1
K-MEANS		76.6	58.4	68.9	37.6	47.9
GMM		75.8	61.9	69.2	36.3	49.4
K-MEDIANS		76.8	58.6	68.8	35.9	40.0
K-MEDOIDS		60.8	58.9	71.3	36.5	46.8
K-MODES		76.2	59.5	71.3	34.2	51.8
KL K-MEANS		76.2	63.3	75.5	39.8	51.2
HSC		9.3	59.2	68.9	28.7	18.1
K-DIRS		81.3	57.7	68.8	FAILS	
K-BETAS		81.1	53.3	51.5	36.7	19.8
K-SBETAS		79.2	<b>65.0</b>	<b>76.6</b>	<b>40.3</b>	<b>56.0</b>

procedures detailed in [44].

**Results.** Table 2 shows interesting comparative results for the real-world softmax predictions scenarios. In the SVHN→MNIST, simplex-tailored methods KL K-MEANS and K-SBETAS clearly stand out from generic methods, both in terms of NMI and Accuracy. In particular, the proposed K-SBETAS achieves the best scores. On the VISDA-C challenge however, KL K-MEANS falls below the baseline similarly to the other state-of-the-art methods. K-DIRS failed to converge. In contrast, K-SBETAS still improves the baseline and presents the best scores. Complementary, we show on Table 3 the running time of these approaches on the same challenges. We can observe that K-SBETAS using MoM parameters estimation presents close or even better running times than the density-EM-based approach GMM. This table also shows that the GPU-based version of K-SBETAS is particularly more interesting on large-scale datasets such as VISDA-C.

**Feature map clustering vs simplex clustering.** On another note, Table 2 interestingly shows that k-means applied on logits points provides equivalent or better scores than k-means applied on bottleneck feature maps. This suggests that the classifier head predicting the logits points does not deteriorate the semantic information inferred from the bottleneck layer. Complementary, Table 3 shows that logits and simplex clustering are less computational demanding than feature map clustering. This is because the simplex points dimension is equal to  $K$ , which is considerably smaller than the feature maps dimension 256 in these cases. In addition, Table 2 shows that proposed simplex clustering method K-SBETAS consistently outperforms the standard K-MEANS feature map clustering, in particular on VISDA-C by a large margin.

Overall, it is worth noting that the explored black-box softmax prediction datasets SVHN→MNIST and VISDA-

TABLE 3: **Computational time** comparison in seconds. All methods are executed on the same hardware: *CPU 11th Gen Intel(R) Core(TM) i7-11700K 3.60GHz*, and *GPU NVIDIA GeForce RTX 2070 SUPER*. MLE-1000 and MLE-500 refer to the MLE parameters estimation with a maximum of 1000 and 500 MLE iterations respectively, while MoM refers the method of moments.

METHOD	SVHN→MNIST ( $N = 10000, K = 10$ )	VISDA-C ( $N = 55388, K = 12$ )
K-MEANS - FEATURE MAP	2.36	18.01
K-MEANS - LOGITS/SIMPLEX	0.06	1.27
GMM	0.43	10.59
K-MEDIANS	5.94	48.39
K-MEDOIDS	8.83	195.00
K-MODES	0.08	4.71
KL K-MEANS	0.27	2.79
HSC	8494.54	>ONE DAY
K-SBETAS (MLE-1000)	64.32	107.43
K-SBETAS (MLE-500)	34.22	58.68
K-SBETAS (MoM)	0.48	3.61
K-SBETAS (MoM, GPU-BASED)	0.13	0.49

C are very challenging in this particular setting. This enables interesting comparisons with state-of-the-art model-agnostic clustering methods. In order to keep the door open for future improvements, we made available these black-box softmax prediction datasets at: [https://github.com/fchiaroni/Clustering\\_Softmax\\_Predictions](https://github.com/fchiaroni/Clustering_Softmax_Predictions). Complementary to these comparative experiments, the next section presents two applications of the competing proposed approach.

## 5.2 Applications

This section conveys the interest of the proposed approach on the applications *One-Shot classification* (Sec. 5.2.1) and *Real-Time UDA segmentation* (Sec. 5.2.2).

### 5.2.1 One-Shot Learning

We consider the One-Shot classification problem, in which a model is evaluated based on its ability to generalize to new classes from a single labelled example per class. Typically, One-Shot methods use the labelled support set  $\mathcal{S}$  of each task to build a classifier and obtain soft predictions for unlabelled query sample. Once soft-predictions have been obtained, proposed K-SBETAS can be used to further refine predictions by clustering soft predictions of the entire query set.

**Setup.** We use two standard benchmarks for One-Shot classification: *mini-Imagenet* [45] and *tiered-Imagenet* [46]. The *mini-Imagenet* benchmark is composed of 60,000 color images [45] equally split among 100 classes, themselves split between train, val and test following [47]. The *tiered-Imagenet* benchmark is a larger dataset with 779,165 images and 608 classes, split following [46]. All images are resized to  $84 \times 84$ . Regarding the networks, we use the pre-trained RN-18 [48] and WRN28-10 [49] provided by [50]. Only 15 unlabeled query data points per class are available during each separate task so we use the biased version of K-SBETAS. As for the methods, we select one inductive method: SimpleSHOT [51] and one transductive method: BD-CSPN [52]. Each One-Shot method is reproduced using

TABLE 4: **1-shot results.** The proposed K-SBETAS further boosts results of existing One-Shot methods by clustering their soft predictions on the query set.

METHOD	NETWORK	<i>mini</i> IMAGENET		<i>tiered</i> IMAGENET	
		(NMI)	(ACC)	(NMI)	(ACC)
SIMPLESHOT	RN-18	49.1	62.7	57.5	69.2
SIMPLESHOT + K-SBETAS	RN-18	<b>52.2</b>	<b>64.4</b>	<b>60.5</b>	<b>71.0</b>
BD-CSPN	RN-18	58.2	68.9	67.2	76.0
BD-CSPN + K-SBETAS	RN-18	<b>60.5</b>	<b>69.8</b>	<b>68.9</b>	<b>76.6</b>
SIMPLESHOT	WRN-28-10	53.6	65.7	59.1	70.4
SIMPLESHOT + K-SBETAS	WRN-28-10	<b>56.8</b>	<b>67.3</b>	<b>61.8</b>	<b>72.4</b>
BD-CSPN	WRN-28-10	62.4	72.1	69.0	77.5
BD-CSPN + K-SBETAS	WRN-28-10	<b>64.0</b>	<b>72.4</b>	<b>70.7</b>	<b>78.3</b>

the set of hyperparameters suggested in the original papers.

**Results.** Table 4 shows that all along these experiments, K-SBETAS consistently improves in terms of NMI and Accuracy scores the output predictions of SimpleSHOT and BD-CSPN.

### 5.2.2 Real-Time UDA for road segmentation

We now consider a question that was, to the best of our knowledge, hitherto unaddressed in UDA segmentation: Can we adapt predictions from a black-box source model on a target set in Real-Time ?

**Setup.** We address this question on the *road* GTA5→*road* Cityscapes challenge. A source model is trained on GTA5 [53], and applied on the Cityscapes validation set [54]. Following [55], we use Deeplab-V2 [56] as the semantic segmentation network. In our case, the model is exclusively trained for the binary task of road segmentation. The validation set contains 500 images, with a 1024\*2048 resolution. In order to simulate a real-time application, we treat each image independently, i.e. as a new clustering task, in which each pixel represents a point to cluster.

**Towards Real-Time running time:** Furthermore, to maximize the speed of execution, we downsample the model’s output probability map prior to fitting the clustering methods, and then use the obtained densities to perform inference at the original resolution. Downsampling in by a factor of 8 allows to increase the frame-rate by almost 2 orders of magnitude, without suffering any mIoU loss<sup>12</sup>. Specifically, K-SBETAS takes in average 0.0165 seconds for clustering on each 128\*256 subset of pixels and 0.0056 seconds for predictions on original 1024\*2048 images, which represents a processing frequency of 45 images per second. Hardware used: CPU 11th Gen Intel(R) Core(TM) i7-11700K 3.60GHz, and GPU NVIDIA GeForce RTX 2070 SUPER.

**Results.** Corresponding NMI and mean IoU scores are displayed on Table 5, and show K-SBETAS outperforming low computational demanding competitors K-MEANS and KL K-MEANS by a large margin, with an improvement of 14 mIoU points over the pixel-wise inductive baseline. Fig. 1 provides qualitative results, in which K-SBETAS yields a definite visual improvement over the baseline. In addition,

TABLE 5: **Real-Time UDA** for road segmentation per image on the challenge GTA5→Cityscapes, by using probability simplex clustering.

APPROACH	GTA5→CITYSCAPES	
	(NMI)	(mIoU)
K-MEANS - LOGITS	21.4	39.4
ARGMAX	19.7	49.2
K-MEANS	23.6	52.4
KL K-MEANS	24.9	52.2
K-SBETAS	<b>35.8</b>	<b>65.7</b>

and consistently with the previous results observed on Table 2 for the UDA classification challenge, Table 5 also shows that clustering the probability simplex points may be more effective than clustering the logits.

### 5.3 Ablation studies

**Joint v.s. Factorised density.** Our proposed method draws inspiration from a factorised Beta density, i.e. each component of the simplex vector is considered independent from each other. While such simplifying assumption has significant analytical and computational benefits, it may also fail to capture the complexity of the target distribution. We explore this trade-off by comparing K-BETAS with K-DIRS, in which the full joint Beta density – corresponding to a Dirichlet density – is fitted at each iteration. Because there exists no closed-form solution to this problem, we resort to the approximate estimation procedure described in [32]. Results in Table 2 show that K-DIRS and K-BETAS produce similar scores on mixtures of Dirichlet distributions. In the meantime, K-DIRS outperforms K-BETAS on SVHN→MNIST but fails to converge on the more challenging VISDA-C challenge, making it ill-suited to real-world applications.

**Effect of class imbalance.** To investigate the problem of class imbalance, we generate heavily imbalanced datasets. First, we create an imbalanced version of our synthetic *Simu* dataset, that we refer to as *iSimu*. Specifically, we weighted the 3 components of the *Simu* mixture with six different combinations using the imbalanced class-proportions {0.75, 0.2, 0.05}. Second, we consider a variant of VISDA-C, where class-proportions are sampled from a Dirichlet distribution with  $\alpha = \mathbf{1}_K$ . We refer to this variant as *iVISDA-Cs*. We perform 10 random re-runs.

Table 6 compares the clustering models on these two datasets. Displayed NMI scores for *iSimu*s correspond to the average NMI scores obtained across the six different mixture proportions. NMI and IoU scores displayed for *iVISDA-Cs* correspond to the average scores obtained across ten different highly imbalanced subsets variants of VISDA-C. K-SBETAS (BIASED) refers to the proposed approach without the marginal probability term  $\pi_k$  in eq. 14. These comparative results clearly highlight the benefit of the proposed K-SBETAS formulation. Note that our unbiased formulation could theoretically apply to metric-based approaches, but was systematically found to produce degenerated solution in which all examples are assigned to a unique cluster.

12. See Table 13 in Appendix for more details.

TABLE 6: Comparative **probability simplex clustering** on highly imbalanced *iSimus* and *iVISDA-Cs* datasets.

APPROACH	iSIMUS	iVISDA-Cs	
	(NMI)	(NMI)	(mIoU)
ARGMAX	55.5	31.6	22.7
K-MEANS	62.3	32.8	24.2
GMM	64.5	34.4	21.1
K-MEDIANS	60.4	33.1	22.4
K-MEDOIDS	62.6	32.1	22.5
K-MODES	55.1	32.0	22.8
KL K-MEANS	59.9	35.2	24.9
HSC	17.7	28.9	16.3
K-SBETAS (BIASED)	55.3	35.4	25.6
K-SBETAS	72.4	36.4	27.1

TABLE 7: Accuracy depending on the unimodal constraint. The constraint is enabled in  $\checkmark$  columns. k-Dirs parameters estimation [32] fails to converge on VISDA-C.

UNIMODAL CONSTRAINT	SVHN $\rightarrow$ MNIST		VISDA-C	
	$\times$	$\checkmark$	$\times$	$\checkmark$
K-DIRS	65.3	<b>68.8</b>	FAILS	FAILS
K-BETAS	19.5	<b>51.5</b>	11.9	<b>19.8</b>
K-SBETAS (MLE-500)	<b>76.2</b>	<b>76.2</b>	<b>55.0</b>	<b>55.0</b>
K-SBETAS	<b>76.6</b>	<b>76.6</b>	<b>56.0</b>	<b>56.0</b>

**Parameters estimation.** Concerning the parameters estimation for K-SBETAS, we can observe on Table 3 and Table 7 that using the method of moments (MoM) is more beneficial than the iterative MLE in practice, both in terms of computational cost and prediction performances.

**Effect of the unimodal constraint.** Table 7 empirically confirms that constraining a density-based clustering model to only consider mixtures of unimodal distributions is appropriate with softmax predictions from pre-trained source models. Yet, we can observe that disabling this constraint has no impact on K-SBETAS results. Such observations are further explained by the presence of  $\delta$  in the following paragraph.

**Effect of  $\delta$ .** As a matter of fact, Table 7 results suggest that  $\delta$  interest is finally twofold in our experiments: It enables a more flexible clustering, meanwhile it can also prevent from estimating bimodal density functions. The latter point can be explained as follow. Bimodal distributions have a higher variance than uniform or unimodal distributions because they partition the major portion of the density at the vicinity of two opposite interval boundaries simultaneously. Thus, when  $\delta$  is sufficiently large (e.g. with  $\delta = 0.15$  in these experiments), the scaled variance of the projection of  $x_i$  coordinates into the interval  $[\frac{\delta}{1+2\delta}, \frac{1+\delta}{1+2\delta}]$  becomes sufficiently small to inhibit the modeling of bimodal distributions. Complementary, Fig. 6 shows that setting  $\delta = 0.15$  provides consistent outperforming results on different datasets and it allows fast convergence in terms of clustering iterations. Thus, we set  $\delta = 0.15$  along all the other presented experiments.

**Pre-clustering: Centroids initialization.** Parameters initialization is notoriously important in unsupervised clustering. On Table 8, we compare the popular k-means++

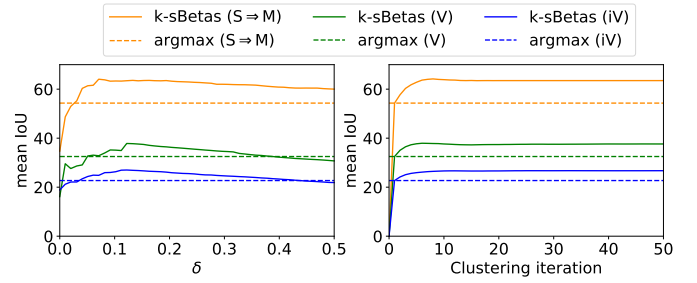


Fig. 6: K-SBETAS mean IoU scores depending on  $\delta$  and on the clustering iteration. We respectively set 25 clustering iterations on the left figure, and  $\delta = 0.15$  on the right one. S $\rightarrow$ M, V and iV respectively refer to SVHN $\rightarrow$ MNIST, VISDA-C, highly imbalanced iVISDA-Cs datasets.

TABLE 8: K-SBETAS prediction performances depending on the parameters initialization and cluster to class assignment. We compare k-means++ with the proposed *vertices init*, and also the centroids assignments argmax with the proposed optimal transport strategy (Hung).

APPROACH	INIT	ASSIGNMENT	SVHN $\rightarrow$ MNIST	VISDA-C
			(ACC)	(ACC)
K-SBETAS	K-MEAN++	ARGMAX	69.0 $\pm$ 6.1	50.0 $\pm$ 5.0
	K-MEANS++	HUNG	69.8 $\pm$ 8.1	47.2 $\pm$ 5.2
	VERTICES	ARGMAX	73.5 $\pm$ 0.0	53.8 $\pm$ 0.0
	VERTICES	HUNG	<b>76.6 <math>\pm</math> 0.0</b>	<b>56.0 <math>\pm</math> 0.0</b>

initialization, designed for generic clustering, and our simplex-tailored vertices init. Regardless of the assignment method, our initialization yields up to 7% improvement in accuracy over k-means++<sup>13</sup>

**Post-clustering: Cluster to class assignment.** We also show on Table 8 the interest of the Hungarian algorithm, referred to as Hung, for the cluster-labels alignment with class-labels. Compared to the argmax assignment for centroids in the context of such closed set challenges, we recall that Hung aims at ensuring that each cluster is assigned to a separate class. We can observe that the proposed Hung strategy is particularly interesting when using the vertices init. This suggests that optimal transport assignment is naturally more relevant with a *good* clustering, i.e. where each cluster is more likely to represent a separate class.

In order to provide a fair comparison with the state-of-the-art, we jointly applied these *pre*- and *post*-clustering strategies on every compared approach.

## 6 DISCUSSION

This section discusses the potential limitations and extensions of the proposed approach.

**Maximum performance may be upper-bounded.** We have shown that clustering softmax predictions with the proposed approach can efficiently improve source model prediction performances, at a reasonable computational footprint. Yet, it is worth noting that we could not reach

<sup>13</sup> Table 12 in Appendix complementary extends this comparison to other clustering approaches. Benefits are similar on every tested approach.



the prediction performances of the recent state-of-the-art self-training [7], which uses to exploit and update the model parameters, from end-to-end along an iterative process. This is because, as for every clustering algorithm, the maximum performance of the proposed approach is upper-bounded by the quality of the output probability simplex domain representation, over which we have no control.

**Spatial analysis could be complementary.** The clustering model does not consider global or local spatial information. That would be worthwhile in challenges such as semantic pixel-wise segmentation to complement it with spatial post-processing techniques [57].

**Clustering softmax predictions for self-training.** All along this article, we have motivated the use of simplex clustering for efficient prediction adjustment of black-box source models. Nevertheless, simplex clustering could also play the role of pseudo-labeling along self-training strategies. This could be a simple and light generic alternative to feature map clustering [16], which would not imply cumbersome manipulation of high-dimensional and hidden feature maps.

**If the number of classes is large.** In some contexts the number of classes  $K$  may be potentially large. For example,  $K$  may correspond to millions of words in neural language modeling. It would be then interesting to envision strategies that reorganize the softmax layer for more efficient calculation [58]. In addition, distortion-based and probabilistic clustering methods usually require a sufficiently large number of points per class to produce a consistent partitioning. Thus, if  $K$  is too large w.r.t. target set size, then the clustering could produce degenerate solutions. It would be interesting to explore hierarchical clustering strategies [59], [60] on the probability simplex domain, as these models can deal with a small amount of data points per class.

**Low-powered devices.** Systems such as mobile robots and embedded systems may not have the resources to perform costly neural network parameters updates on the application time. The presented framework can be viewed as an efficient plug-in solution for prediction adjustment in the wild when using such low-powered devices.

## 7 CONCLUSION

In this paper, we have tackled the simplex clustering of softmax predictions from black-box deep networks. We found that existing distortion-based objectives of the state-of-the-art do not enable to properly approximate real-world simplex distributions, which can be for example highly peaked at the simplex vertices. Thus, we have introduced a novel probabilistic clustering objective that integrates a generalization of the Beta density, which we coin *sBeta*. This scaled variant of Beta is relatively more permissive, meanwhile we constrain it to fit only strictly uni-modal distributions and to avoid degenerate solutions. In order to optimize our clustering objective, we proceed with a block-coordinate descent approach, which alternates optimization w.r.t assignment variables and parameters estimations of cluster distributions, s.t. the introduced parameters constraints.

The resulting clustering model, that we refer to as *K-SBETAS*, is both highly competitive and efficient on the proposed simulated and real-world softmax-prediction datasets, including class-imbalance scenarios, along which we performed our comparisons. Complementary, we emphasized the interest of simplex clustering throughout two practical applications: One-shot image classification, and Real-Time adjustment for road segmentation on full-size images.

Perspectives are to spread probability simplex clustering insights on other challenges such as pseudo-labeling for self-training procedures, and on additional applications requiring fast correction of source models. Moreover, it may be interesting to complement the clustering with spatial and temporal information depending on the target data properties.

Overall, we hope that the presented simplex clustering framework and softmax-prediction benchmarks will encourage the community to give more attention to such facilitating, low-computational demanding, model-agnostic, plug-in solutions.

## ACKNOWLEDGMENTS

This research was supported by computational resources provided by Compute Canada.

## REFERENCES

- [1] L. Liu, W. Ouyang, X. Wang, P. Fieguth, J. Chen, X. Liu, and M. Pietikäinen, "Deep learning for generic object detection: A survey," *International journal of computer vision*, vol. 128, no. 2, pp. 261–318, 2020.
- [2] Y. Cui, R. Chen, W. Chu, L. Chen, D. Tian, Y. Li, and D. Cao, "Deep learning for image and point cloud fusion in autonomous driving: A review," *IEEE Transactions on Intelligent Transportation Systems*, 2021.
- [3] S. Minaee, Y. Y. Boykov, F. Porikli, A. J. Plaza, N. Kehtarnavaz, and D. Terzopoulos, "Image segmentation using deep learning: A survey," *IEEE transactions on pattern analysis and machine intelligence*, 2021.
- [4] J. Quiñero-Candela, M. Sugiyama, A. Schwaighofer, and N. D. Lawrence, *Dataset shift in machine learning*. MIT Press, 2008.
- [5] D. Wang, E. Shelhamer, S. Liu, B. Olshausen, and T. Darrell, "Tent: Fully test-time adaptation by entropy minimization," in *International Conference on Learning Representations*, 2021.
- [6] M. Wang and W. Deng, "Deep visual domain adaptation: A survey," *Neurocomputing*, vol. 312, pp. 135–153, 2018.
- [7] J. Liang, D. Hu, Y. Wang, R. He, and J. Feng, "Source data-absent unsupervised domain adaptation through hypothesis transfer and labeling transfer," *IEEE Transactions on Pattern Analysis and Machine Intelligence*, 2021.
- [8] K. Muhammad, A. Ullah, J. Lloret, J. D. Ser, and V. H. C. de Albuquerque, "Deep learning for safe autonomous driving: Current challenges and future directions," *IEEE Transactions on Intelligent Transportation Systems*, vol. 22, no. 7, pp. 4316–4336, 2021.
- [9] A. Shrestha and A. Mahmood, "Review of deep learning algorithms and architectures," *IEEE access*, vol. 7, pp. 53 040–53 065, 2019.
- [10] H. Xia, H. Zhao, and Z. Ding, "Adaptive adversarial network for source-free domain adaptation," in *Proceedings of the IEEE/CVF International Conference on Computer Vision (ICCV)*, October 2021, pp. 9010–9019.
- [11] G. Ateniese, L. V. Mancini, A. Spognardi, A. Villani, D. Vitali, and G. Felici, "Hacking smart machines with smarter ones: How to extract meaningful data from machine learning classifiers," *International Journal of Security and Networks*, vol. 10, no. 3, pp. 137–150, 2015.
- [12] F. Pereira, N. Tishby, and L. Lee, "Distributional clustering of english words," *arXiv preprint cmp-lg/9408011*, 1994.
- [13] A. Banerjee, S. Merugu, I. S. Dhillon, J. Ghosh, and J. Lafferty, "Clustering with bregman divergences," *Journal of machine learning research*, vol. 6, no. 10, 2005.

- [14] J. Wu, H. Xiong, and J. Chen, "Sail: Summation-based incremental learning for information-theoretic clustering," in *Proceedings of the 14th ACM SIGKDD international conference on knowledge discovery and data mining*, 2008, pp. 740–748.
- [15] K. Chaudhuri and A. McGregor, "Finding metric structure in information theoretic clustering," in *COLT*, vol. 8. Citeseer, 2008, p. 10.
- [16] M. Caron, P. Bojanowski, A. Joulin, and M. Douze, "Deep clustering for unsupervised learning of visual features," in *Proceedings of the European Conference on Computer Vision (ECCV)*, 2018, pp. 132–149.
- [17] F. Nielsen and K. Sun, "Clustering in hilbert's projective geometry: The case studies of the probability simplex and the ellipsope of correlation matrices," in *Geometric Structures of Information*. Springer, 2019, pp. 297–331.
- [18] R. O. Duda, P. E. Hart, and D. G. Stork, *Pattern Classification*, 2nd ed. John Wiley and Sons, 2000.
- [19] D. Aloise, A. Deshpande, P. Hansen, and P. Popat, "Np-hardness of euclidean sum-of-squares clustering," *Machine Learning*, vol. 75, no. 2, pp. 245–248, 2009.
- [20] P. S. Bradley, O. L. Mangasarian, and W. N. Street, "Clustering via concave minimization," *Advances in neural information processing systems*, pp. 368–374, 1997.
- [21] M. A. Carreira-Perpinán and W. Wang, "The k-modes algorithm for clustering," *arXiv preprint arXiv:1304.6478*, 2013.
- [22] I. M. Ziko, E. Granger, and I. B. Ayed, "Scalable laplacian k-modes," in *Neural Information Processing Systems (NeurIPS)*, 2018, pp. 10 062–10 072.
- [23] A. Krause, P. Perona, and R. Gomes, "Discriminative clustering by regularized information maximization," *Advances in neural information processing systems*, vol. 23, 2010.
- [24] D. J. Rezende, S. Mohamed, and D. Wierstra, "Stochastic backpropagation and approximate inference in deep generative models," in *International conference on machine learning*. PMLR, 2014, pp. 1278–1286.
- [25] W. Hu, T. Miyato, S. Tokui, E. Matsumoto, and M. Sugiyama, "Learning discrete representations via information maximizing self-augmented training," in *International conference on machine learning*. PMLR, 2017, pp. 1558–1567.
- [26] S. Claiici, M. Yurochkin, S. Ghosh, and J. Solomon, "Model fusion with kullback-leibler divergence," in *International Conference on Machine Learning*. PMLR, 2020, pp. 2038–2047.
- [27] T. F. Gonzalez, "Clustering to minimize the maximum intercluster distance," *Theoretical computer science*, vol. 38, pp. 293–306, 1985.
- [28] R. Panigrahy and S. Vishwanathan, "Ano ( $\log^* n$ ) approximation algorithm for the asymmetric-center problem," *Journal of Algorithms*, vol. 27, no. 2, pp. 259–268, 1998.
- [29] Y. Boykov, H. Isack, C. Olsson, and I. Ben Ayed, "Volumetric bias in segmentation and reconstruction: Secrets and solutions," in *IEEE International Conference on Computer Vision (ICCV)*, 2015, pp. 1769–1777.
- [30] M. Tang, D. Marin, I. B. Ayed, and Y. Boykov, "Kernel cuts: Kernel and spectral clustering meet regularization," *International Journal of Computer Vision*, vol. 127, no. 5, pp. 477–511, 2019.
- [31] M. Kearns, Y. Mansour, and A. Y. Ng, "An information-theoretic analysis of hard and soft assignment methods for clustering," in *Learning in graphical models*. Springer, 1998, pp. 495–520.
- [32] T. Minka, "Estimating a dirichlet distribution," 2000.
- [33] M. J. Wainwright, M. I. Jordan *et al.*, "Graphical models, exponential families, and variational inference," *Foundations and Trends® in Machine Learning*, vol. 1, no. 1–2, pp. 1–305, 2008.
- [34] J. Kruschke, *Doing Bayesian data analysis: A tutorial with R, JAGS, and Stan*. Academic Press, 2014.
- [35] D. Arthur and S. Vassilvitskii, "k-means++: The advantages of careful seeding," Stanford, Tech. Rep., 2006.
- [36] O. Bachem, M. Lucic, S. H. Hassani, and A. Krause, "Approximate k-means++ in sublinear time," in *Thirtieth AAAI conference on artificial intelligence*, 2016.
- [37] H. W. Kuhn, "The hungarian method for the assignment problem," *Naval research logistics quarterly*, vol. 2, no. 1-2, pp. 83–97, 1955.
- [38] C. Biernacki, G. Celeux, and G. Govaert, "Assessing a mixture model for clustering with the integrated completed likelihood," *IEEE transactions on pattern analysis and machine intelligence*, vol. 22, no. 7, pp. 719–725, 2000.
- [39] L. Kaufman and P. J. Rousseeuw, "Partitioning around medoids (program pam)," *Finding groups in data: an introduction to cluster analysis*, vol. 344, pp. 68–125, 1990.
- [40] Y. Cheng, "Mean shift, mode seeking, and clustering," *IEEE transactions on pattern analysis and machine intelligence*, vol. 17, no. 8, pp. 790–799, 1995.
- [41] Y. Netzer, T. Wang, A. Coates, A. Bissacco, B. Wu, and A. Y. Ng, "Reading digits in natural images with unsupervised feature learning," in *NIPS Workshop*, 2011.
- [42] Y. LeCun, L. Bottou, Y. Bengio, and P. Haffner, "Gradient-based learning applied to document recognition," *Proceedings of the IEEE*, vol. 86, no. 11, pp. 2278–2324, 1998.
- [43] X. Peng, B. Usman, N. Kaushik, D. Wang, J. Hoffman, and K. Saenko, "Visda: A synthetic-to-real benchmark for visual domain adaptation," in *Proceedings of the IEEE Conference on Computer Vision and Pattern Recognition Workshops*, 2018, pp. 2021–2026.
- [44] J. Liang, D. Hu, and J. Feng, "Do we really need to access the source data? source hypothesis transfer for unsupervised domain adaptation," in *International Conference on Machine Learning*. PMLR, 2020, pp. 6028–6039.
- [45] O. Vinyals, C. Blundell, T. Lillicrap, D. Wierstra *et al.*, "Matching networks for one shot learning," *Advances in neural information processing systems*, vol. 29, pp. 3630–3638, 2016.
- [46] M. Ren, E. Triantafillou, S. Ravi, J. Snell, K. Swersky, J. B. Tenenbaum, H. Larochelle, and R. S. Zemel, "Meta-learning for semi-supervised few-shot classification," in *International Conference on Learning Representations ICLR*, 2018.
- [47] S. Ravi and H. Larochelle, "Optimization as a model for few-shot learning," in *International Conference on Learning Representations ICLR*, 2017.
- [48] K. He, X. Zhang, S. Ren, and J. Sun, "Deep residual learning for image recognition," in *Proceedings of the IEEE conference on computer vision and pattern recognition*, 2016, pp. 770–778.
- [49] S. Zagoruyko and N. Komodakis, "Wide residual networks," *arXiv preprint arXiv:1605.07146*, 2016.
- [50] M. Boudiaf, Z. I. Masud, J. Rony, J. Dolz, P. Piantanida, and I. B. Ayed, "Transductive information maximization for few-shot learning," *arXiv preprint arXiv:2008.11297*, 2020.
- [51] Y. Wang, W.-L. Chao, K. Q. Weinberger, and L. van der Maaten, "Simpleshot: Revisiting nearest-neighbor classification for few-shot learning," *arXiv preprint arXiv:1911.04623*, 2019.
- [52] J. Liu, L. Song, and Y. Qin, "Prototype rectification for few-shot learning," in *Computer Vision—ECCV 2020: 16th European Conference, Glasgow, UK, August 23–28, 2020, Proceedings, Part I 16*. Springer, 2020, pp. 741–756.
- [53] S. R. Richter, V. Vineet, S. Roth, and V. Koltun, "Playing for data: Ground truth from computer games," in *European conference on computer vision*. Springer, 2016, pp. 102–118.
- [54] M. Cordts, M. Omran, S. Ramos, T. Rehfeld, M. Enzweiler, R. Benenson, U. Franke, S. Roth, and B. Schiele, "The cityscapes dataset for semantic urban scene understanding," in *Proceedings of the IEEE Conference on Computer Vision and Pattern Recognition (CVPR)*, June 2016.
- [55] T.-H. Vu, H. Jain, M. Bucher, M. Cord, and P. Pérez, "Advent: Adversarial entropy minimization for domain adaptation in semantic segmentation," in *Proceedings of the IEEE/CVF Conference on Computer Vision and Pattern Recognition*, 2019, pp. 2517–2526.
- [56] L.-C. Chen, G. Papandreou, I. Kokkinos, K. Murphy, and A. L. Yuille, "Deepplab: Semantic image segmentation with deep convolutional nets, atrous convolution, and fully connected crfs," *IEEE transactions on pattern analysis and machine intelligence*, vol. 40, no. 4, pp. 834–848, 2017.
- [57] V. Badrinarayanan, A. Kendall, and R. Cipolla, "Segnet: A deep convolutional encoder-decoder architecture for image segmentation," *IEEE transactions on pattern analysis and machine intelligence*, vol. 39, no. 12, pp. 2481–2495, 2017.
- [58] W. Chen, D. Grangier, and M. Auli, "Strategies for training large vocabulary neural language models," in *Proceedings of the 54th Annual Meeting of the Association for Computational Linguistics (Volume 1: Long Papers)*. Berlin, Germany: Association for Computational Linguistics, Aug. 2016, pp. 1975–1985.
- [59] F. Murtagh and P. Contreras, "Algorithms for hierarchical clustering: an overview," *Wiley Interdisciplinary Reviews: Data Mining and Knowledge Discovery*, vol. 2, no. 1, pp. 86–97, 2012.
- [60] G. Ahalya and H. M. Pandey, "Data clustering approaches survey and analysis," in *2015 International Conference on Futuristic Trends on Computational Analysis and Knowledge Management (ABLAZE)*. IEEE, 2015, pp. 532–537.



**Florent Chiaroni** is currently a postdoctoral fellow at ÉTS Montreal, Canada and Institut National de la Recherche Scientifique (INRS), Montreal, Canada. He received his Dipl-Ing degree in computer science and electronics from ESTIA, Bidart, France, in 2016 and his M.Sc. degree in robotics and embedded systems from the University of Salford Manchester, United Kingdom, in 2016. He received his Ph.D. degree in signal and image processing from the University of Paris Saclay in 2020, with VEDECOM Institute,

Versailles, France, and Université Paris-Saclay, Centre national de la recherche scientifique (CNRS), CentraleSupélec, Gif-Sur-Yvette, France. His current research interests include clustering and efficient weakly-supervised learning for pattern analysis.



**Malik Boudiaf** is a PhD candidate at ÉTS Montréal, Canada, supervised by Prof. Ismail Ben Ayed and Prof. Pablo Piantanida. He obtained his MSc in Aeronautics & Astronautics from Stanford University in 2019, and his M.Eng in Aerospace Engineering from ISAE-Supaero, France in 2017. His current research interests lie between Computer Vision, Information Theory and Optimization, and their application to few-shot/unsupervised learning.



**Amar Mitiche** holds the Licence Es Sciences degree in mathematics from the University of Algiers and the Ph.D. degree in computer science from the University of Texas at Austin. He is currently a Professor with the Department of Telecommunications (INRS-EMT), Institut National de la Recherche Scientifique (INRS), Montreal, QC, Canada. His research is in computer vision and pattern recognition. He has written several articles on the subjects, as well as three books: Computational Analysis of Visual Motion (Plenum

Press, 1994), Variational and Level Set Methods in Image Segmentation (Springer, 2011), with Ismail Ben Ayed, and Computer Vision Analysis of Image Motion by Variational Methods (Springer, 2014), with J. K. Aggarwal. His current interests include image segmentation, image motion analysis, and pattern classification by neural networks.



**Ismail Ben Ayed** is currently a Full Professor at ÉTS Montreal. He is also affiliated with the CRCHUM. His interests are in computer vision, optimization, machine learning and medical image analysis algorithms. Ismail authored over 100 fully peer-reviewed papers, mostly published in the top venues of those areas, along with 2 books and 7 US patents. In the recent years, he gave over 30 invited talks, including 4 tutorials at flagship conferences (MICCAI'14, ISBI'16, MICCAI'19 and MICCAI'20). His research has been covered

in several visible media outlets, such as Radio Canada (CBC), Quebec Science Magazine and Canal du Savoir. His research team received several recent distinctions, such as the MIDL'19 best paper runner-up award and several top-ranking positions in internationally visible contests. Ismail served as Program Committee for MICCAI'15, MICCAI'17 and MICCAI'19, and as Program Chair for MIDL'20. Also, he serves regularly as reviewer for the main scientific journals of his field, and was selected several times among the top reviewers of prestigious conferences (such as CVPR'15 and NEURIPS'20).





	sBETA	BETA
DENSITY FUNCTION	$f_{\text{sBeta}} = \frac{(x + \delta)^{\alpha-1}(1 + \delta - x)^{\beta-1}}{B(\alpha, \beta)(1 + 2\delta)^{\alpha+\beta-2}}$	$f_{\text{Beta}} = \frac{x^{\alpha-1}(1 - x)^{\beta-1}}{B(\alpha, \beta)}$
MEAN (SEC. A.1)	$E_{sB}[X] = \frac{\alpha}{\alpha + \beta}(1 + 2\delta) - \delta$	$E_B[X] = \frac{\alpha}{(\alpha + \beta)}$
VARIANCE (SEC. A.1)	$V_{sB}[X] = \frac{\alpha\beta}{(\alpha + \beta)^2(\alpha + \beta + 1)}(1 + 2\delta)^2$	$V_B[X] = \frac{\alpha\beta}{(\alpha + \beta)^2(\alpha + \beta + 1)}$
MODE (SEC. A.2)	$m_{sB} = \frac{\alpha - 1 + \delta(\alpha - \beta)}{\alpha + \beta - 2}$	$m_B = \frac{\alpha - 1}{\alpha + \beta - 2}$
CONCENTRATION (SEC. 4.2.3)	$\lambda = \alpha + \beta - 2$	$\lambda = \alpha + \beta - 2$
METHOD OF MOMENTS (SEC. 4.3)	$\alpha = \left( \frac{\mu_\delta(1 - \mu_\delta)(1 + 2\delta)^2}{V_{sB}[X]} - 1 \right) \mu_\delta$ $\beta = \left( \frac{\mu_\delta(1 - \mu_\delta)(1 + 2\delta)^2}{V_{sB}[X]} - 1 \right) (1 - \mu_\delta),$ $\text{WITH } \mu_\delta = \frac{E_{sB}[X] + \delta}{1 + 2\delta}$	$\alpha = \left( \frac{E_B[X](1 - E_B[X])}{V_B[X]} - 1 \right) E_B[X]$ $\beta = \left( \frac{E_B[X](1 - E_B[X])}{V_B[X]} - 1 \right) (1 - E_B[X])$

## A.2 Mode

The mode of a density function  $f(x)$  corresponds to the value of  $x$  at which  $f(x)$  achieves its maximum.

$$\begin{aligned}
& -2\delta \int (x + \delta) f_{\text{sBeta}}(x) dx \\
& = -2\delta \int \underbrace{\frac{(x + \delta)^{(\alpha+1)-1} (1 + \delta - x)^{\beta-1}}{B(\alpha, \beta) (1 + 2\delta)^{\alpha+\beta-2}}}_{= E_{sB}[X] + \delta = \frac{\alpha}{\alpha+\beta} (1 + 2\delta) \text{ using Eq. (23)}} dx \quad (27) \\
& = -2\delta \frac{\alpha}{\alpha + \beta} (1 + 2\delta).
\end{aligned}$$

Finally, we can estimate the variance (i.e., the second central moment)  $V_{sB}[X]$ , as a function of sBeta density parameters, using Eq. (23) and Eq. (25) as follow:

$$\begin{aligned}
V_{sB}[X] &= E_{sB}[X^2] - E_{sB}[X]^2 \\
&= \frac{(\alpha+1)\alpha}{(\alpha+1+\beta)(\alpha+\beta)}(1+2\delta)^2 \\
&\quad - 2\delta \frac{\alpha}{\alpha+\beta}(1+2\delta) + \delta^2 \\
&\quad - \left[ \frac{\alpha}{\alpha+\beta}(1+2\delta) - \delta \right]^2 \\
&= \frac{\alpha\beta}{(\alpha+\beta)^2(\alpha+\beta+1)}(1+2\delta)^2.
\end{aligned} \tag{28}$$

**Linear property:** With respect to the expectation linearity, it is worth noting that we have  $\frac{E[X]+\delta}{1+2\delta} = E\left[\frac{X+\delta}{1+2\delta}\right]$  and

$$\begin{aligned} V\left[\frac{X+\delta}{1+2\delta}\right] &= E\left[\left(\frac{X+\delta}{1+2\delta} - E\left[\frac{X+\delta}{1+2\delta}\right]\right)^2\right] \\ &= \frac{E[(X-E[X])^2]}{(1+2\delta)^2} \\ &= \frac{V[X]}{(1+2\delta)^2}. \end{aligned} \quad (29)$$

$$\begin{aligned}
f'_{\text{sBeta}}(x) &= \frac{df_{\text{sBeta}}(x)}{dx} = \frac{d}{dx} \frac{(x+\delta)^{\alpha-1}(1+\delta-x)^{\beta-1}}{B(\alpha, \beta)(1+2\delta)^{\alpha+\beta-2}} \\
&= \frac{1}{B(\alpha, \beta)(1+2\delta)^{\alpha+\beta-2}} \frac{d}{dx} (x+\delta)^{\alpha-1}(1+\delta-x)^{\beta-1} \\
&= \frac{(\alpha-1)(x+\delta)^{\alpha-2}(1+\delta-x)^{\beta-1}}{B(\alpha, \beta)(1+2\delta)^{\alpha+\beta-2}} \\
&\quad - \frac{(x+\delta)^{\alpha-1}(\beta-1)(1+\delta-x)^{\beta-2}}{B(\alpha, \beta)(1+2\delta)^{\alpha+\beta-2}}.
\end{aligned} \tag{30}$$

Then, we can solve  $\frac{df_{\text{sBeta}}(x)}{dx} = 0$  as follow:

$$\begin{aligned} \frac{df_{\text{sBeta}}(x)}{dx} &= 0 \\ \Rightarrow (\alpha - 1)(x + \delta)^{\alpha-2}(1 + \delta - x)^{\beta-1} \\ &\quad - (x + \delta)^{\alpha-1}(\beta - 1)(1 + \delta - x)^{\beta-2} = 0 \quad (31) \\ \Rightarrow (\alpha - 1)(1 + \delta - x) - (\beta - 1)(x + \delta) &= 0 \\ \Rightarrow x &= \frac{\alpha - 1 + \delta(\alpha - \beta)}{\alpha + \beta - 2}. \end{aligned}$$

Thus, the mode of sBeta with  $\alpha, \beta > 1$  is defined as  $m_{sB} = \frac{\alpha-1+\delta(\alpha-\beta)}{\alpha+\beta-2}$ .

### A.3 Solving the necessary conditions for minimizing the objective w.r.t sBeta parameters

Let us compute the partial derivatives of our objective  $L_{\text{sBeta}}$  (14) for  $\alpha_{k,n}$  and  $\beta_{k,n}$ :

$$\begin{aligned}\frac{\partial L_{\text{sBeta}}}{\partial \alpha_{k,n}} &= \sum_{i=1}^N u_{i,k} \log(x_{i,n} + \delta) - \left( \sum_{i=1}^N u_{i,k} \right) \log(1 + 2\delta) \\ &\quad - \left( \sum_{i=1}^N u_{i,k} \right) (\psi(\alpha_{k,n}) - \psi(\alpha_{k,n} + \beta_{k,n})) \\ \frac{\partial L_{\text{sBeta}}}{\partial \beta_{k,n}} &= \sum_{i=1}^N u_{i,k} \log(1 + \delta - x_{i,n}) - \left( \sum_{i=1}^N u_{i,k} \right) \log(1 + 2\delta) \\ &\quad - \left( \sum_{i=1}^N u_{i,k} \right) (\psi(\beta_{k,n}) - \psi(\alpha_{k,n} + \beta_{k,n}))\end{aligned}\tag{32}$$

where  $\psi$  stands for the di-gamma function. Setting partial derivatives in (32) to 0 leads to the following coupled system:

$$\begin{aligned}\alpha_{k,n} &= \psi^{-1}(\psi(\alpha_{k,n} + \beta_{k,n}) \\ &\quad + \frac{1}{\sum_{i=1}^N u_{i,k}} \sum_{i=1}^N u_{i,k} \log(\frac{x_{i,n} + \delta}{1 + 2\delta})) \\ \beta_{k,n} &= \psi^{-1}(\psi(\alpha_{k,n} + \beta_{k,n}) \\ &\quad + \frac{1}{\sum_{i=1}^N u_{i,k}} \sum_{i=1}^N u_{i,k} \log(\frac{1 + \delta - x_{i,n}}{1 + 2\delta}))\end{aligned}\tag{33}$$

While (33) does not have any analytical solution, we approximate updates in (33) by fixing the right hand side of each equation, leading the following vectorized updates of parameters  $\alpha_k$  and  $\beta_k$  for each cluster  $k$ :

$$\alpha_k^{(t+1)} = \psi^{-1}(\psi(\alpha_k^{(t)} + \beta_k^{(t)})\tag{34}$$

$$+ \frac{1}{\sum_{i=1}^N u_{i,k}} \sum_{i=1}^N u_{i,k} \log(\frac{\mathbf{x}_i + \delta}{1 + 2\delta}))\tag{35}$$

$$\beta_k^{(t+1)} = \psi^{-1}(\psi(\alpha_k^{(t)} + \beta_k^{(t)})\tag{36}$$

$$+ \frac{1}{\sum_{i=1}^N u_{i,k}} \sum_{i=1}^N u_{i,k} \log(\frac{1 + \delta - \mathbf{x}_i}{1 + 2\delta}))$$

We empirically validated such optimization procedure converged to the MLE estimate on synthetically generated dataset.

## APPENDIX B

### SUPPLEMENTARY EXPERIMENTS

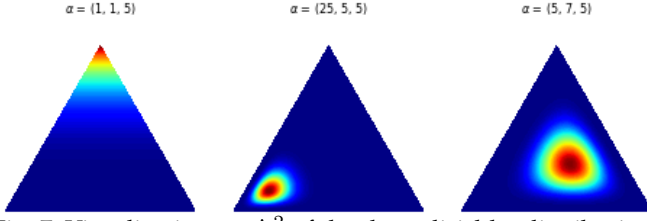


Fig. 7: Visualization on  $\Delta^2$  of the three dirichlet distributions used to generate random artificial datasets *Simu* and *iSimus*, introduced in Sec. 5.

TABLE 10: Balanced clustering on *Simu* depending on the dataset size.

DATASET SIZE APPROACH	100 000 (NMI)	10 000 (NMI)	1 000 (NMI)	100 (NMI)
ARGMAX	60.1 $\pm$ 0.5	59.8 $\pm$ 0.7	60.4 $\pm$ 3.9	62.0 $\pm$ 17.9
K-MEANS	76.6 $\pm$ 0.1	76.7 $\pm$ 0.5	76.9 $\pm$ 6.2	78.2 $\pm$ 21.8
KL K-MEANS	76.2 $\pm$ 0.2	76.3 $\pm$ 0.7	76.5 $\pm$ 6.2	78.1 $\pm$ 22.8
GMM	75.8 $\pm$ 0.3	75.8 $\pm$ 1.2	75.9 $\pm$ 6.8	77.3 $\pm$ 28.4
K-MEDIANS	76.8 $\pm$ 0.1	77.1 $\pm$ 0.7	77.1 $\pm$ 5.6	78.7 $\pm$ 22.2
K-MEDOIDS	60.8 $\pm$ 14.4	64.2 $\pm$ 12.1	65.3 $\pm$ 19.4	71.8 $\pm$ 24.2
K-MODES	76.2 $\pm$ 0.2	76.3 $\pm$ 1.0	76.5 $\pm$ 5.3	77.5 $\pm$ 24.9
HSC	9.3 $\pm$ 1.9	15.0 $\pm$ 2.7	30.6 $\pm$ 16.3	41.2 $\pm$ 27.9
K-SBETAS	<b>79.5 <math>\pm</math> 0.1</b>	<b>79.5 <math>\pm</math> 0.8</b>	<b>79.8 <math>\pm</math> 6.4</b>	<b>80.0 <math>\pm</math> 25.4</b>

TABLE 11: Imbalanced clustering on *iSimus* depending on the dataset size.

DATASET SIZE APPROACH	100 000 (NMI)	10 000 (NMI)	1 000 (NMI)
ARGMAX	55.5 $\pm$ 25.5	55.6 $\pm$ 26.8	55.6 $\pm$ 31.5
K-MEANS	62.3 $\pm$ 22.6	62.2 $\pm$ 23.4	62.4 $\pm$ 28.9
KL K-MEANS	59.9 $\pm$ 25.2	59.9 $\pm$ 26.0	60.2 $\pm$ 31.5
GMM	60.6 $\pm$ 23.9	63.8 $\pm$ 29.3	63.9 $\pm$ 35.0
K-MEDIANS	60.4 $\pm$ 24.8	60.3 $\pm$ 25.6	60.3 $\pm$ 32.2
K-MEDOIDS	47.2 $\pm$ 33.0	55.4 $\pm$ 30.0	57.8 $\pm$ 35.9
K-MODES	55.1 $\pm$ 30.9	54.9 $\pm$ 32.4	54.8 $\pm$ 36.5
HSC	17.7 $\pm$ 12.1	13.6 $\pm$ 11.7	29.1 $\pm$ 31.8
K-SBETAS	<b>72.4 <math>\pm</math> 17.2</b>	<b>72.2 <math>\pm</math> 20.1</b>	<b>73.3 <math>\pm</math> 29.2</b>

TABLE 12: **k-means++** versus **vertices init** (proposed). Balanced clustering on softmax predictions. Performances are averaged over ten executions. Note that k-means++ is stochastic while the vertices init is not.

DATASET INITIALIZATION APPROACH	SVHN $\rightarrow$ MNIST		VISDA-C	
	K-MEANS++ (ACC)	VERTICES INIT (ACC)	K-MEANS++ (ACC)	VERTICES INIT (ACC)
K-MEANS	66.6 $\pm$ 5.4	<b>68.9 <math>\pm</math> 0.0</b>	44.5 $\pm$ 3.3	<b>47.9 <math>\pm</math> 0.0</b>
KL K-MEANS	72.6 $\pm$ 7.8	<b>75.5 <math>\pm</math> 0.0</b>	50.0 $\pm$ 2.7	<b>51.2 <math>\pm</math> 0.0</b>
GMM	60.6 $\pm$ 9.6	<b>69.2 <math>\pm</math> 0.0</b>	43.8 $\pm$ 5.2	<b>49.4 <math>\pm</math> 0.0</b>
K-MEDIANS	67.4 $\pm$ 9.2	<b>68.8 <math>\pm</math> 0.0</b>	38.5 $\pm$ 4.0	<b>40.0 <math>\pm</math> 0.0</b>
K-MEDOIDS	51.9 $\pm$ 4.9	<b>71.3 <math>\pm</math> 0.0</b>	40.6 $\pm$ 8.6	<b>46.8 <math>\pm</math> 0.0</b>
K-MODES	60.6 $\pm$ 13.0	<b>71.3 <math>\pm</math> 0.0</b>	30.2 $\pm$ 6.3	<b>31.1 <math>\pm</math> 0.0</b>
K-SBETAS	69.8 $\pm$ 8.1	<b>76.6 <math>\pm</math> 0.0</b>	47.2 $\pm$ 5.2	<b>56.0 <math>\pm</math> 0.0</b>

TABLE 13: **Running time** of K-SBETAS (GPU-based) on *GT45 road*  $\rightarrow$  *Cityscapes road* depending on the subset size. This GPU-based implementation uses the pytorch library. We fixed to 10 the maximum number of K-SBETAS clustering iterations. We assume that the segmentation model and K-SBETAS method run on the same GPU, i.e. no loading time implied by the softmax prediction set. CPU used: 11th Gen Intel(R) Core(TM) i7-11700K 3.60GHz. GPU used: NVIDIA GeForce RTX 2070 SUPER. Presented prediction scores were all obtained on the full size (1024\*2048) set.

SUBSET SIZE	RUNNING TIME (SECONDS)		FULL SIZE SCORES	
	(CLUSTERING)	(PREDICTION)	(NMI)	(mIoU)
FULL SIZE (1024*2048)	0.2784	0.0056	35.8	65.7
MODULO 2 (512*1024)	0.0812	0.0019	35.8	65.7
MODULO 4 (256*512)	0.0282	0.0009	35.8	65.7
MODULO 8 (128*256)	0.0165	0.0004	35.8	65.7

TABLE 14: **iVISDA-Cs imbalanced proportions.** In order to obtain 10 imbalanced subsets of VISDA-C that we refer to *iVISDA-Cs*, we have randomly generated ten random vectors from a dirichlet distribution. VISDA-C contains 12 classes, so the dimension of this dirichlet distribution is equal to 12. Dirichlet parameters are set as  $\alpha = \{\alpha_n = 1\}_{n=1}^{D=12}$ , such that this dirichlet distribution is uniform on  $\Delta^{11}$ . Below is the list of the ten sets of rounded proportions obtained, and the corresponding number of examples for each VISDA-C class. For every class, examples from the original dataset are always picked in the same order, by starting at the beginning of the target image list of VISDA-C.

CLASSES	PLANE	BCYCL	BUS	CAR	HORSE	KNIFE	MCYCL	PERSON	PLANT	SKTBRD	TRAIN	TRUCK
VISDA-C PROPORTIONS	0.0658	0.0627	0.0847	0.1878	0.0847	0.0375	0.1046	0.0722	0.0821	0.0412	0.0765	0.1002
NUMBER OF EXAMPLES	3646	3475	4690	10401	4691	2075	5796	4000	4549	2281	4236	5548
PROPORTIONS SET 1	0.0406	0.2315	0.0953	0.0257	0.2367	0.0443	0.0930	0.0252	0.1347	0.0601	0.0012	0.0116
NUMBER OF EXAMPLES	275	1568	645	173	1603	300	630	170	912	407	8	78
PROPORTIONS SET 2	0.0996	0.0234	0.0086	0.0112	0.1490	0.0064	0.1900	0.1223	0.1287	0.0387	0.0876	0.1346
NUMBER OF EXAMPLES	675	158	58	75	1009	43	1286	828	871	262	593	912
PROPORTIONS SET 3	0.0511	0.1170	0.0779	0.0661	0.0127	0.0575	0.0166	0.1958	0.0047	0.0795	0.2147	0.1064
NUMBER OF EXAMPLES	346	792	527	448	85	389	112	1326	31	538	1454	720
PROPORTIONS SET 4	0.1382	0.0014	0.1726	0.0017	0.0030	0.1600	0.2470	0.0726	0.0419	0.0524	0.0558	0.0534
NUMBER OF EXAMPLES	936	9	1169	11	20	1084	1673	492	284	354	378	361
PROPORTIONS SET 5	0.0013	0.0227	0.1451	0.1049	0.2725	0.0511	0.0196	0.0500	0.1401	0.0193	0.0322	0.1411
NUMBER OF EXAMPLES	8	154	983	710	1846	346	132	338	948	130	218	956
PROPORTIONS SET 6	0.1450	0.0202	0.0343	0.1604	0.0574	0.0183	0.0318	0.0368	0.2668	0.0356	0.1361	0.0570
NUMBER OF EXAMPLES	982	137	232	1086	388	123	215	249	1807	241	922	386
PROPORTIONS SET 7	0.1200	0.1304	0.0310	0.0451	0.0308	0.0071	0.1194	0.2701	0.0122	0.1311	0.0911	0.0116
NUMBER OF EXAMPLES	812	883	209	305	208	48	809	1830	82	888	617	78
PROPORTIONS SET 8	0.0166	0.0521	0.0457	0.0358	0.1175	0.1917	0.0258	0.2303	0.1503	0.0379	0.0600	0.0362
NUMBER OF EXAMPLES	112	352	309	242	796	1298	174	1560	1018	256	406	245
PROPORTIONS SET 9	0.1523	0.1316	0.0196	0.0427	0.0380	0.0806	0.0423	0.2075	0.0383	0.0644	0.1074	0.0754
NUMBER OF EXAMPLES	1031	891	132	289	257	546	286	1405	259	436	727	510
PROPORTIONS SET 10	0.0102	0.1336	0.0063	0.0131	0.1291	0.0812	0.0019	0.0967	0.3063	0.0770	0.1107	0.0337
NUMBER OF EXAMPLES	69	905	42	88	874	549	12	655	2074	521	750	228



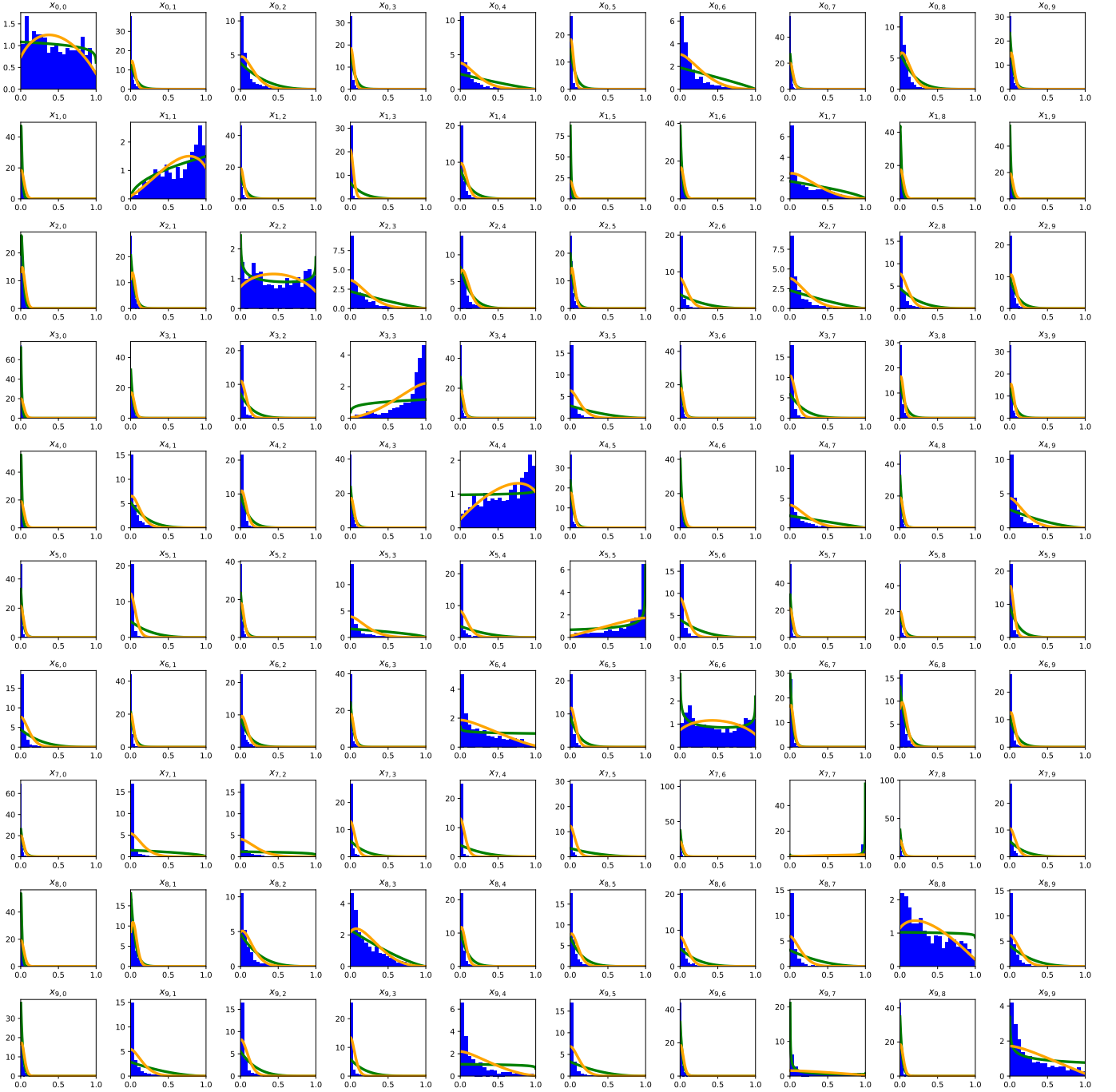


Fig. 8: Histograms per coordinate of softmax predictions obtained on MNIST, with a source model pre-trained on SVHN. Rows correspond to softmax predictions for a given class. Columns refer to the softmax predictions coordinates. Green curves represent Beta density estimations and orange curves represent sBeta density estimations. *We invite the reader on the pdf version to zoom on these vectorized figures.*

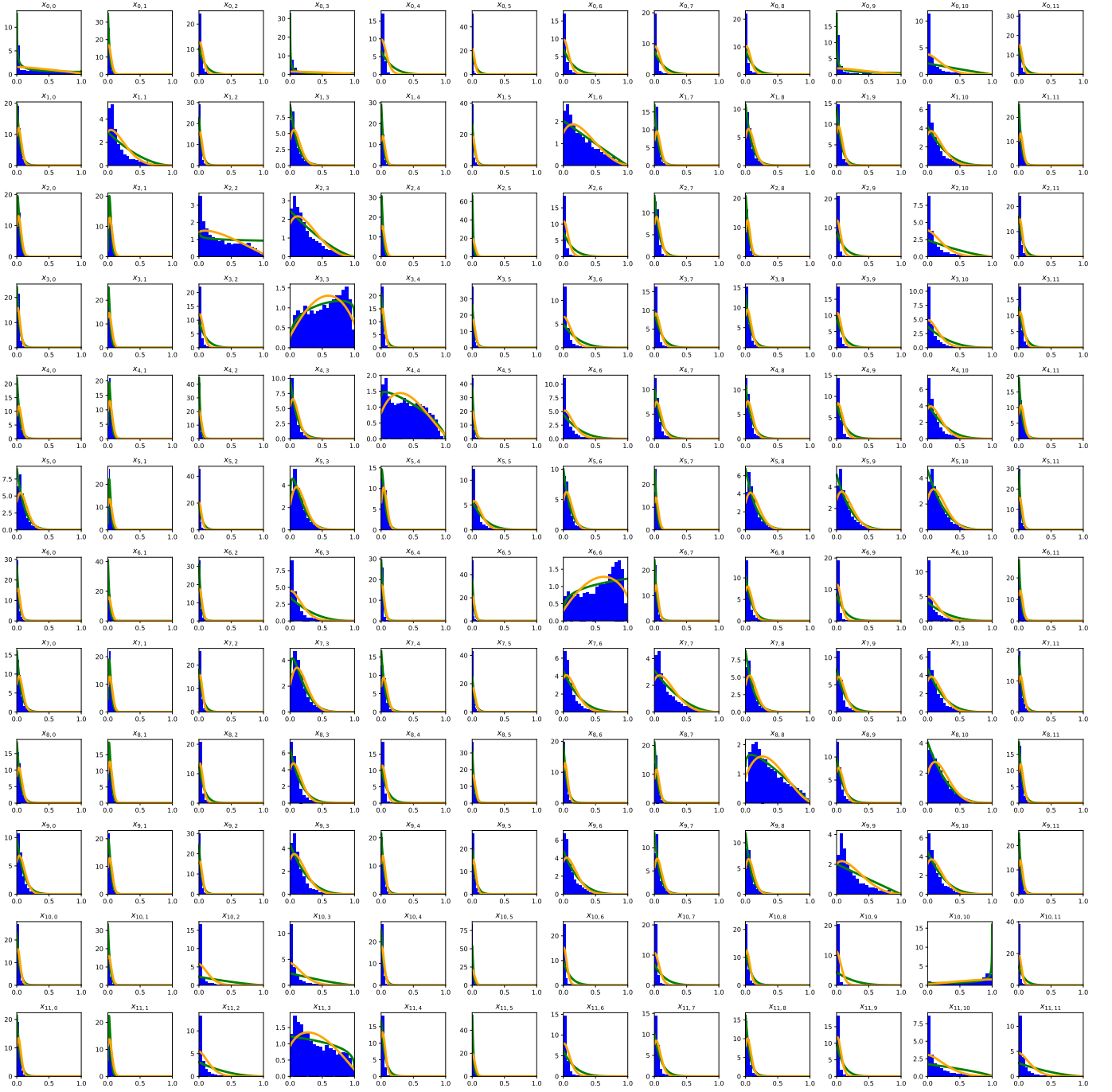


Fig. 9: Histograms per coordinate of softmax predictions on the challenge VISDA-C. Rows correspond to softmax predictions for a given class. Columns refer to softmax predictions coordinates. Green curves represent Beta density estimations and orange curves represent sBeta density estimations. *We invite the reader on the pdf version to zoom on these vectorized figures.*